Montanuniversitaet Leoben

Development of micrometer-sized specimen production processes for nonconductive materials

Diploma thesis at the
Institute of Material Physics, Montanuniversitaet
Leoben, Austria

Leoben, June 2014 Gabor Milassin

EIDESSTATTLICHE ERKLÄRUNG

Ich erkläre an Eides statt, dass ich diese Arbeit selbstständig verfasst, andere als die angegebenen Quellen und Hilfsmittel nicht benutzt und mich auch sonst keiner unerlaubten Hilfsmittel bedient habe.

AFFIDAVIT

I declare in lieu of oath, that I wrote this thesis and performed the associated research myself, using only literature cited in this volume.

Date Signature

Development of micrometer-sized specimen production processes for nonconductive materials

The position resolved measurement of mechanical properties of materials allows a mapping of inhomogeneities and enables us to draw conclusions about the local composition, damage evolution and microstructure. The motivation for this work came from the prospect of gaining a better insight into the ageing mechanisms of fluorinated ethylene propylene (FEP) in low earth orbit (LEO) environment, which can lead to severe embrittlement of the polymer. FEP is widely used in form of foils for the outermost layer of the multi layer insulation (MLI) of spacecrafts. In this function, FEP is exposed directly to the LEO environment. The aim was to produce flat tensile specimens with a thickness of a few tens of micrometers, to be able to resolve a possible gradient in the mechanical properties within the 127 µm thick FEP outer layer of MLI, which was retrieved from the Hubble Space Telescope. Various types of micro machining methods were tested and assessed. The use of a microtome and an ion milling system proved to give the best results in respect to cheap and relatively fast specimen production. The well reproducible specimens were tested in tensile tests under an optical microscope and the results were then complemented by spectroscopic measurements.

Entwicklung eines Probenfertigungsverfahrens für nichtleitende Materialien mit Abmessungen im Mikrometerbereich

Durch die Messung der mechanischen Eigenschaften eines Materials in Abhängigkeit der Probenentnahmeposition können Rückschlüsse auf Inhomogenitäten in der Werkstoffzusammensetzung, räumlich begrenzte Schädigungen beziehungsweise auf die lokale Mikrostruktur gezogen werden. Die Motivation zur vorliegenden Arbeit ist ein genaueres Verständnis der Alterungsmechanismen von Perfluorethylenpropylen-Copolymer (FEP) in der niedrigen Erdumlaufbahn (LEO), die zur starken Versprödung des Materials führen können. FEP wird in Form von Folien als äußerste Schicht der passiven thermischen Multilagen-Isolation (MLI) von Satelliten verwendet und wird in dieser Anwendung direkt den Einflüssen im LEO ausgesetzt. Ziel war es Flachzugproben mit einer Dicke in der Größenordnung von einigen zehn Mikrometern herzustellen. Damit soll an im Orbit gealterten Material des Hubble Weltraumteleskops ein durch Alterung entstandener etwaiger Gradient in den mechanischen Eigenschaften der 127 µm dicken FEP MLI Außenschicht bestimmt werden. Es wurden verschiedene Bearbeitungsmethoden experimentell getestet, bewertet und ein günstiges und relativ schnelles Präparationsverfahren, welches den Einsatz eines Mikrotoms und eines Ionenpolierers vorsieht, entwickelt. Die gut reproduzierbaren Proben wurden unter einem Lichtmikroskop im Zugversuch getestet und die Ergebnisse durch spektroskopische Untersuchungen ergänzt.

Acknowledgements

First of all I would like to thank my supervisors Univ. Prof. Dr. Reinhard Pippan, Director of the Erich Schmid Institute of Materials Science of the Austrian Academy of Sciences and Dr. Stefan Wurster, for supporting me in doing my thesis.

Furthermore I wish to thank Dipl.-Ing. Dr. Christopher Semprimoschnig, my supervisor at the European Space Technology and Research Centre (TEC-QTE), especially for assigning me this project.

In addition I would like to thank Dipl.-Ing. Dr. Gernot Oreski, from the Polymer Competence Center Leoben, where the ATR-IR measurements were carried out.

I am also indebted to Dipl.-Ing. Katharina Bruckmoser and Dipl.-Ing. Florian Arbeiter from the Department of Polymer Technology at the Montanuniversitaet Leoben. I would like to thank them for conducting the Raman measurements, their advices about sample preparation and for the organisation of the laser ablation test at the research group of laser micromachining of materials at the University of Salamanca, Spain.

Moreover I wish to thank all the staff of the Erich Schmid Institute, for their hospitality, help and all the good times with them.

Finally I would like to thank my family and friends for their love, friendship and support.

Contents

1 Introduction

Spacecraft need to withstand a multitude of environmental influences to ensure the functionality of their payload over the expected operational lifetime. To ensure this, materials used on the outer layer are chosen especially for their robustness and protective function against the harsh environment of space. In Low Earth Orbit (LEO) and Geo Synchronous Orbit (GEO) metallised Fluorinated Ethylene Propylene (FEP) has been used widespread as a passive thermal control material. FEP was used as second-surface-mirror-material also on the Hubble Space Telescope (HST - Figure 1.1), where it showed signs of degradation on several solar facing surfaces.

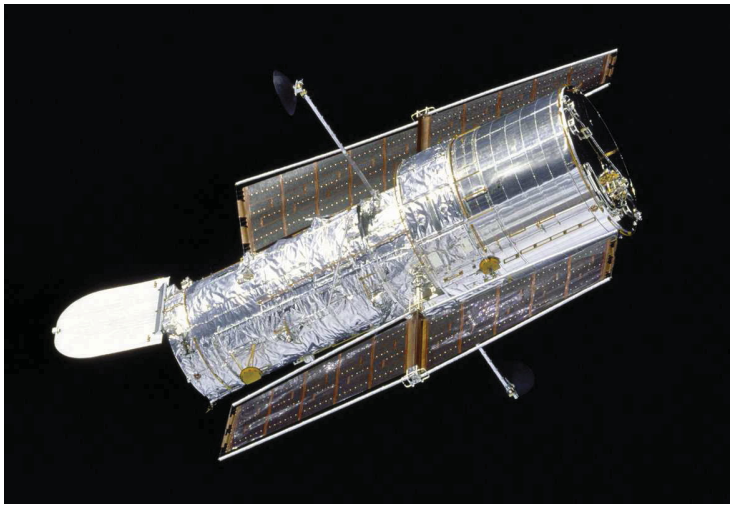

Figure 1.1: The Hubble Space Telescope [1]

The ageing of FEP was researched extensively (see section 1.2.1) especially after discovery of discolouration and through thickness cracks have been observed on the outer layer of the HST by the crew of the second servicing mission (see Figure 1.2). Investigation of samples retrieved from orbit and of specimen aged on-ground in simulated space environments gave an insight into the governing ageing mechanisms and their influence on the thermo-optical and mechanical properties of FEP. The existence of a strongly embrittled surface layer on the solar facing side of space-exposed material was suggested, but till now only techniques probing the whole thickness of the foil were available.

The aim of this work was to develop a sample preparation technique, enabling the sampling and subsequent tensile testing of nonconductive materials such as polymers - particularly FEP - with a specimen thickness of a few tens of micrometers. The goal was to achieve a through thickness mapping of mechanical properties with a spatial resolution in the same order of magnitude. This new preparation technique should contribute to the understanding of in orbit ageing of FEP.

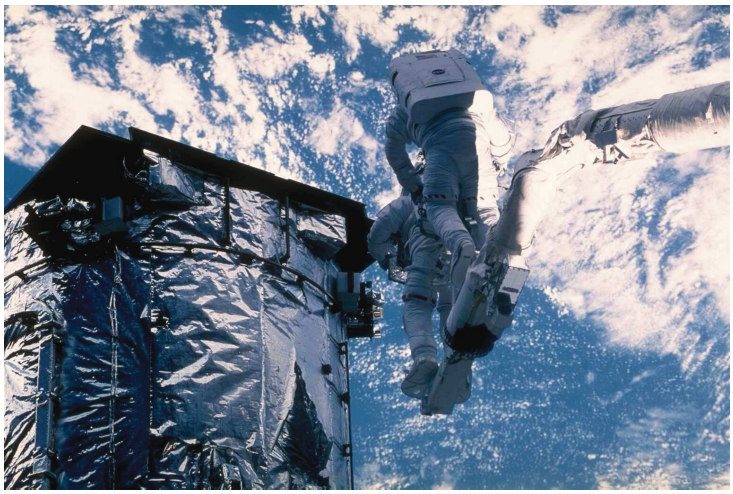

Figure 1.2: Two through thickness cracks in the HST MLI as observed during servicing mission 2 in February 1997 [2]

The feasibility of different machining techniques was assessed with virgin Teflon®[i] FEP foil samples. Single processing tests were carried out with a focussed ion beam (FIB) system and a femtosecond laser. Utilising a microtome and an ion milling system a parameter study was started to find the procedure leading to the best results regarding sample quality and reproducibility. After the first well reproducible specimens could be prepared, a tensile test set-up used for copper samples was adapted for testing FEP. Force-displacement curves were recorded, stress-strain curves were calculated and compared to previous results from macroscopic foil tensile specimens. Foil samples aged in LEO - retrieved from the HST - were machined and tested according to the developed procedures. The use of a graphical software tool made it possible to match the individual specimens to their sampling depth within the original foil sample. Finally, it was possible to plot data obtained from the tensile tests versus the sampling depth. Further investigations, using surface sensitive spectroscopic tools, as attenuated total reflectance (ATR) infrared (IR) spectroscopy and confocal Raman microspectroscopy, applied on thin sections of aged material were implemented.

The project was carried out at the Erich Schmid Institute of Materials Science (ESI) in cooperation with the Department of Polymer Engineering and Science at the Montanuniversität Leoben, Austria. The research was funded and the samples were provided by the European Space Technology and Research Centre (ESTEC) Noordwijk, The Netherlands.

[i] Teflon is a registered trademark of E.I. duPont de Nemours & Co., Wilmington, DE, USA

1.1 The Hubble Space Telescope

The feasibility of placing automated telescopes into Earth orbit was examined the first time in a report by Lyman Spitzer in 1946 [3] - more than ten years before the launch of Sputnik 1, the first successful artificial Earth satellite. The main motivation for using Earth-bound satellites for space exploration is the possibility of observing radiation from space without having to look through our planets blurring and wavelength-specifically absorbing atmosphere. The HST is not the first space located automated telescope but it is the biggest science research satellite so far in many senses. With costs at launch of 1.5 billion Dollars, a length of 13.2 m, a total mass of more than 11 tons and an operational time of over 24 years the HST represents probably the biggest step in astronomy since the discovery of the first refractor telescope [1]. It helped to reveal the age of the universe more accurately than ever before, played an important role in the discovery of dark energy and changed our view of the universe, as did Edwin Hubble's findings, which provided the basis for the Big Bang theory and whom the HST was named after. Not to be forgotten, the HST also helped to awaken the fascination to space also to non-astronomers by providing high resolution images of distant objects.

The HST is a joint project from the National Aeronautics and Space Administration (NASA) and the European Space Agency (ESA). ESA contributed subsystems like the Faint Object Camera, the original power supply system including the two Solar Array Drive Mechanisms and the belonging control electronics which turned the photo voltaic generators towards the Sun without disturbing the pointing accuracy of the HST. The cooperation means also, that ESA therefore gets access to 15 % of the observing time [4].

The history and design of the HST were strongly connected to the operation of the Space Transportation System (STS) with its Orbiter Vehicles (OV), the Space Shuttles [5]. This reusable low Earth orbital spacecraft was chosen to place the HST into a circular orbit in approximately 600 km hight and an inclination of 28.5° relative to the equator [4]. The launch with the STS determined the satellite's maximal mass, size, orbital altitude and provided the possibility of in orbit servicing missions. The later option made it possible to repeatedly prolong the mission and update the instruments and subsystems regularly.

Soon after placing the HST into its orbit on 24 April 1990, a spherical aberration of the main mirror was found to blur the images it sent back to Earth. The defect could be reconstructed perfectly, which enabled the development of the Corrective Optics Space Telescope Axial Replacement (COSTAR). COSTAR was designed to replace the High Speed Photometer and to achieve the originally intended high resolution for all remaining instruments on board of the HST. During the first servicing mission in December 1993 COSTAR and a new pair of solar arrays (called SA2) were installed besides the replacement of many other sub systems. HST's second servicing mission took place in February 1997, where again many units were changed for new or refurbished ones [4]. During that mission also severe degradation of some thermal control materials was detected (see Figure 1.2). Many cracks were patched and a tightly curled up piece of MLI was returned for on ground inspection [2]. Later, the replacement of thermal control materials got an integral part of servicing missions. The tasks of the scheduled third mission was split into two parts, SM3A and SM3B, after three of HST's six error-prone gyroscopes failed. This number is required for the attitude control of the HST. SM3A took place in December 1999, a bit more than a

month after the failure of the fourth gyroscope, which made it necessary to set the satellite into safe mode. However, maintenance work of SM3A restored the full operational capability of HST. During SM3B, in March 2002, the HST noticeably changed its appearance, as the old solar arrays (SA2) were replaced by smaller rigid ones. Servicing mission 4 - the fifth and last STS mission to the HST - took place in May 2009. All crucial subsystems were maintained to prolong HST's operational lifetime through 2014 and the so-called Soft Capture Mechanism was installed to facilitate an autonomous rendezvous with a de-orbiting satellite [4].

Most of Hubble's outer surface is covered with thermal control materials, mainly MLI blankets and radiator surfaces (see Figure 1.1). Both layered materials use a 127 µm (0.005") Teflon® FEP foil as a space-exposed layer with a metallized second surface reflective layer. For the MLI, vapour deposited aluminium (VDA) with a thickness of about 100 nm was used (FEP/VDA). Behind this first layer 15 layers of embossed 8.17 µm (0.00033") double-aluminized Kapton®[ii] and an innermost layer with 24.5 µm (0.001") single aluminized Kapton® were used. For the radiator surfaces perforated self-adhesive silver Teflon® tape was directly bonded to the HST's aluminium substrate. Its reflective layer was made of roughly 100 nm vapour deposited silver (VDS), protected by an Inconel coating and finally coated with an acrylic adhesive [6]. MLI material similar to the one described above was utilized for the protection of the solar array drive arms (SADA, see figure 1.3) of the under ESA responsibility built solar arrays [7].

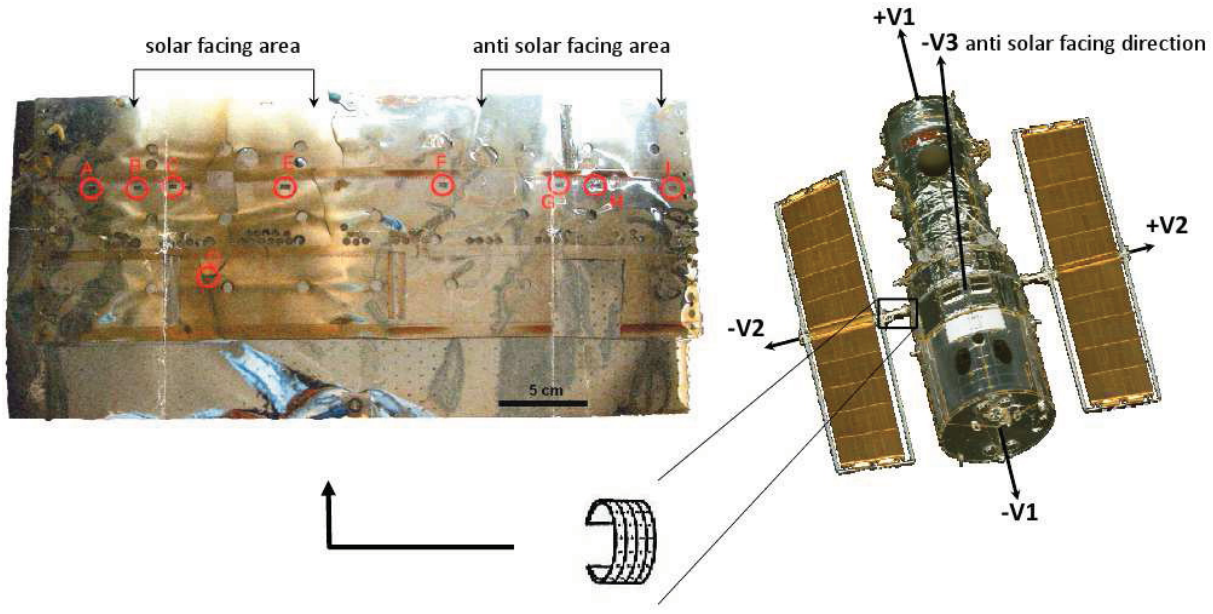

Figure 1.3: The position of the SADA MLI retrieved from HST in March 2002 is shown. The red circles with adjacent red capital letters are marking the sampling position of the foil samples received for this work. The positions where the main focus is lead on during tensile testing are A, B, C and D, representing solar-facing and solar-grazing angles [8].

[ii] Kapton is a registered trademark of E.I. duPont de Nemours & Co., Wilmington, DE, USA

1.1.1 Low Earth Orbit Environment

The Earth's atmosphere varies with altitude in composition, density and temperature, so the transition to outer space is fluent. Nevertheless, a hight of 100 km above the ground is referred to as the boundary to space in aeronautics. At about that hight, the so called Karman line, air craft would need to increase their speed to compensate for the exponentially decaying density of atmosphere (to keep aerodynamic lifting forces constant) till a speed, where they reach the circular orbital speed of that hight. From that moment on no aerodynamic forces are necessary, since centrifugal forces are taking over [9]. At the lower edge of the thermosphere, around 80 km above sea level, the composition of the atmosphere's gas mixture starts to change dramatically from mainly molecular nitrogen and oxygen towards its photolysis products generated by the Sun's UV light, atomic oxygen (AO) and atomic nitrogen. From that point on, the atmosphere's temperature is increasing with the altitude due to the interaction with short wave length solar radiation and the hot plasma of the solar wind at high geographic latitudes. Orbits around Earth can be divided into three zones with different environmental influences. LEO is defined to extend 1000 km above sea level and is the lowest possible and easiest accessible orbit. Mid Earth Orbit is located between 1000 km and 35,000 km and Geosynchronous Orbit is situated around 36,000 km [10].

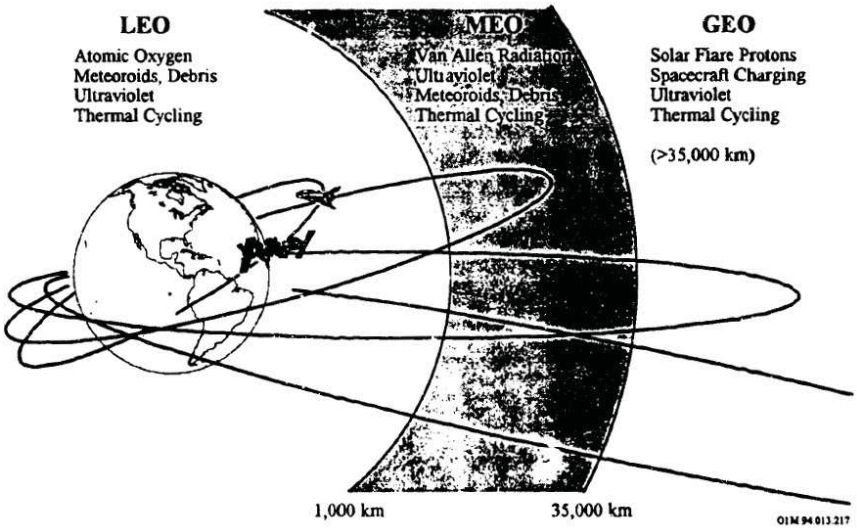

Figure 1.4: Variation of space environments with altitude [11]

To describe the surrounding of spacecraft in LEO one should focus on the by far biggest source of energy in our solar system, the Sun. The yellow-dwarf star of our solar system can be described fundamentally as a giant thermonuclear fusion reactor with a surface temperature of ~5800 K, radiating with a spectrum similar to black body radiation. The discrepancies relative to a spectrum based merely on the Sun's surface temperature arise from the solar atmosphere, which is responsible for enhanced emission in the ultraviolet (UV) region. In figure 1.5, the deviation from a smooth curve shape is clearly visible. Additionally to electromagnetic radiation, the Sun also produces a steady flux of plasma driven outwards by the Sun's radiation pressure. This fluence is called solar wind and interacts with Earth's magnetic fields. The LEO environment is largely shielded from the solar wind, but charged particles are trapped within the magnetosphere forming van Allen belts in a region $\pm 50°$ geomagnetic latitude. In a region called the South Atlantic Anomaly, the van Allen belt reaches down to an altitude of less than 500 km and therefore affects also the

orbit of the HST with omnidirectional electron and proton radiation [10] [11] [12]. Further, during high solar activity also a significant amount of X-rays are emitted from solar flares. By integrating the solar spectrum over all wavelengths, the total irradiated energy per unit area can be calculated. At a distance of one astronomical unit (AU = average distance between Earth and Sun, $1.496 \cdot 10^8$ km) this is equal to 1366 W/m^2 [13] and called the solar constant. Only 7% of the Sun's energy is irradiated in the UV wavelengths ($\lambda < 380$ nm). However, this radiation plays an important role in the ageing of polymers, as it possesses enough energy to break atomic bonds in organic materials (see figure 1.6).

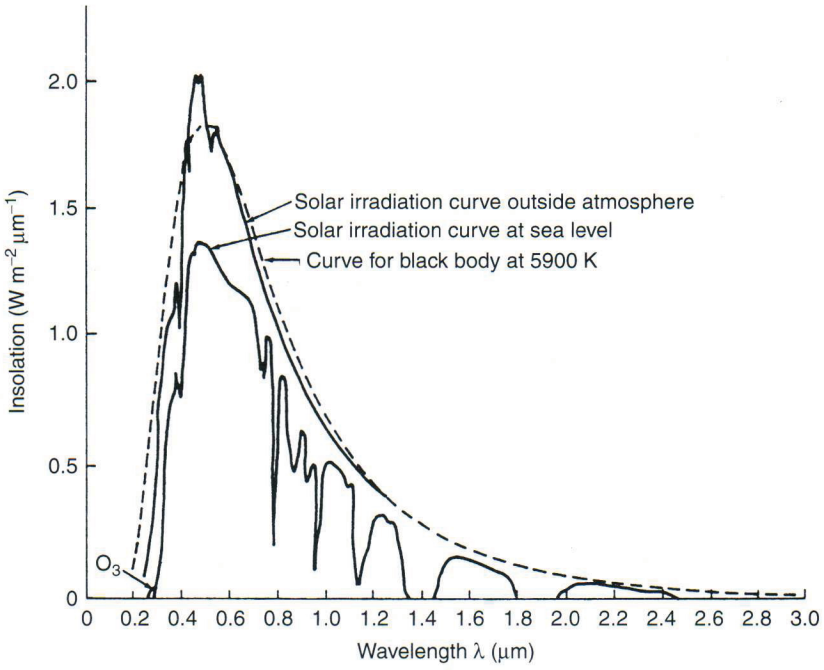

Figure 1.5: Comparison of solar spectra in space and on earth with black body radiation [10]

Besides the Sun, a satellite in LEO is receiving radiation energy from the Earth: by the diffuse radiation reflected from incoming solar radiation (with a reflectivity called the Earth albedo) and the outgoing thermal radiation emitted by the Earth and its atmosphere (named Earth shine). This means, that also material on the anti-solar facing side of the satellite receives radiation while completing a whole orbit. Satellites in LEO also regularly pass through the Earth's shadow, yielding to a regular change in irradiation intensities. For quantifying the solar exposure in this surroundings the term equivalent sun hours (ESH) is used, which equals the number of hours of direct sunlight needed to yield to the same total dose of sunlight. The changes in irradiation are also leading to thermal cycling, whereby one orbital period (96 minutes for the HST) is leading to one

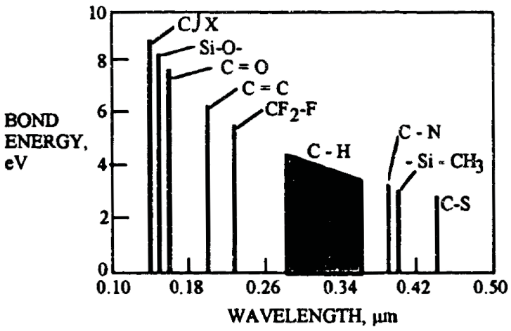

Figure 1.6: Wavelength requirements to break various polymeric bonds [11]

thermal cycle .

Large amounts of objects in the size range of a few microns to a few meters are existing in orbits around Earth, which are called meteoroids if their origin is non-man-made and orbital debris if they were brought into orbit during space missions. With respect to the meteoroids, the primary threat is from particles ranging from 50 µm to 1 mm diameter (micrometeoroids) as those can already cause damage and penetrate the spacecraft's MLI. The collision speeds can vary widely, depending on the impact vector and the orbital speed of the spacecraft. The mean value for collisions is estimated at about 19 km/s [11]. Up to an altitude of 2000 km, where most spacecraft are operated, space debris is affecting the environment on a higher scale than micrometeoroids. Particles in the range of 10^{-3} to 10^{-9} g have a high enough flux to erode surfaces and penetrate protective coatings [10]. To limit the source of future space debris, ESA defined rules for its own future missions, including the de-orbit of all satellites within an altitude of 2000 km within 25 years after the end of their operational time [14].

Summarizing up, at the orbital altitude of the HST solar exposure, plasma exposure, solar event X-rays, thermal cycling, atomic oxygen, micrometeoroids and debris are the main factors affecting the spacecraft [10]. The calculated environmental impacts on the SADA MLI exposed 8,25 years to LEO are listed in table 1.1.

Exposure	SM1 to SM3B
ESH, Solar facing	46,028 h
ESH, Anti-solar facing	14,330 h
Thermal cycles	45,000
Temperature range	$\pm$ 100°C
X-ray fluence 1 - 8 Å	< 355.8 J/m^2
X-ray fluence 0.5 - 4 Å	< 22.6 J/m^2
Electron fluence > 40 keV	$< 3.89 \cdot 10^{13}$ e$^-$ cm^{-2}
Proton fluence > 40 keV	$< 3.84 \cdot 10^{10}$ e$^-$ cm^{-2}
AO fluence solar facing	$2.7 \cdot 10^{20}$ atoms/cm^2
AO fluence anti-solar facing	$3.4 \cdot 10^{20}$ atoms/cm^2

Table 1.1: Exposure conditions for HST SADA surfaces [8]

1.1.2 Heat transfer in space

Transferring thermal energy in the vacuum of space is possible only via thermal radiation, which is a non material bound way of energy transfer. Spacecraft are heated by the Sun, albedo, Earth shine and by internal power dissipation. On the other hand surfaces, which are not facing the sun are radiating heat away. As spacecraft in LEO are subjected to an extremely changing temperature environment, it is important to shield its components from extreme temperatures and keep the subsystems within their qualified operational temperature limits (e. g. -15°C to +50°C for electronic equipment) by thermal control systems [10].
A surface can reflect, absorb and transmit incoming radiation and emit its own heat energy by thermal radiation. The fractions of incoming radiation which are reflected are called reflectance ρ, the fraction absorbed absorptance α and the fraction transmitted transmittance τ.

$$\begin{aligned} Q &= Q\rho + Q\alpha + Q\tau \\ 1 &= \rho + \alpha + \tau \end{aligned} \tag{1.1}$$

Outer surfaces can be treated as grey body emitters, radiating a fraction ϵ of the radiation of a black body at the same temperature and may be expressed as

$$q = \epsilon\sigma T^4$$

where q is the total radiated energy per unit surface area, σ is the Stefan-Boltzmann constant ($5.67 \cdot 10^{-8}$ $Wm^{-2}K^{-4}$) and T is the absolute temperature in Kelvin. It is not possible to emit higher amounts of energy at a certain temperature than a black body, so that the value of ϵ lies always between 0 and 1 ($=$ black body). This results in the fundamental parameters establishing the thermal radiation balance at a certain temperature being: the amount of externally and internally absorbed heat, and the ratio of solar absorptance to infrared emittance (α/ϵ) of external surfaces.
The spectral wavelength dependency of the black body radiation is described mathematically by the Planck equation

$$E_{\lambda,T} = \frac{8\pi hc}{\lambda^5} \frac{1}{e^{\frac{hc}{\lambda k_B T}} - 1}$$

where h is Planck's constant ($6.626 \cdot 10^{-34}$ Js), c is the speed of light ($2.998 \cdot 10^{8}$ m/s), λ is the wavelength (m), k_B is the constant of Boltzmann ($1.381 \cdot 10^{-23}$ J/K) and T is the Temperature [15]. In figure 1.5 it can be seen, that for a temperature of 5900 K, the surface temperature of the sun, the wavelength band of emittance is concentrated in the region between 0.2 and 3µm. Maximal emission occurs according to Wien's displacement law at

$$\lambda_{max} = \frac{b}{T}$$

where λ_{max} is the peak wavelength (m), b is Wien's displacement constant ($2.898 \cdot 10^{-3}$ mK) [16]. For the Sun λ is in the visible wavelength around 500 nm, but for objects at room temperature (RT = 293 K) the peak emission wavelength can be found at about 9.8 µm. So, solar radiation is concentrated in a rather small wavelength band at short wavelengths, while emission at RT is spread over a long wavelength region of the IR band.
The radiative heat exchange between two surfaces is characterised by three important parameters: the surface temperatures, surface properties and the view factor. The radiative view factor F_{12} is defined as the fraction of the radiation leaving one surface and intercepted

by another [10]. This factor is needed to assess the amount of radiation received from an external source like the albedo, or also from components of the spacecraft itself. Mathematically the view factor between two diffuse surfaces of the area A_1 and A_2 can be described by

$$F_{12} = \frac{1}{A_1} \int_{A_1} \int_{A_2} \frac{cos\phi_1 cos\phi_2}{\pi s^2} \mathrm{d}A_1 \, \mathrm{d}A_2.$$

Angles ϕ_1 and ϕ_2 are angles between the surface normals and the connection line between the two surfaces, as depicted in figure 1.7.

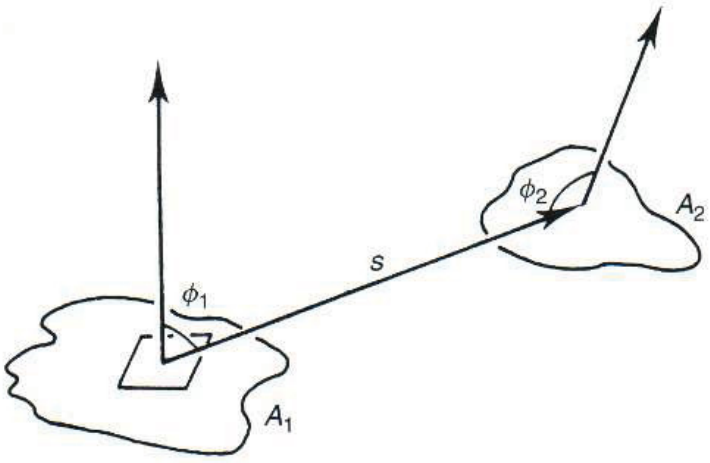

Figure 1.7: View factor geometry between surfaces A_1 and A_2 [10]

Finally the equilibrium temperature at the surface of a spacecraft can be calculated by expressing the conditions for a balance between heat input and output:

$$A_{SC}\epsilon\sigma T^4 = A_S\alpha Q_S + A_P\alpha Q_A + A_P\epsilon F_{12} Q_P + Q_i$$

where A_{SC} is the surface area of the spacecraft (m^2), A_S and A_P are the projected areas of the spacecraft (m^2) in the direction of the Sun and the planet, Q_S, Q_A and Q_P are irradiation intensities from the Sun, albedo and planetary thermal radiation (W/m^2), and Q_i is the internal power dissipation of the spacecraft (W/m^2) [7]. This equation describes the output of thermal energy by the spacecraft on the left side and the input from various heat sources on the right side, being the solar radiation, albedo, planetary radiation and internal heat sources. A rough estimation of the spacecraft's outer layer temperature can be carried out by using averaged irradiation values over a whole orbital cycle.

1.1.3 Passive thermal control

As described above, the incoming sun radiation and the outgoing thermal emittance at RT are covering different wavelength regions, giving the possibility of engineering the α/ϵ value of spacecraft surfaces by combining materials with different thermo-optical properties. For good insulation first of all a big portion of the incoming radiation has to be reflected, to limit the heat energy input to the system. This requirement leads directly to a low absorptance α because spacecraft do not allow transmittance in the UV-Vis-IR region and thus equation 1.1 results to

$$\alpha = 1 - \rho.$$

Finally high reflectance is necessary to cool surfaces effectively via heat radiation. For the thermal control of spacecraft both, specular and diffuse reflectors with low α and high emittance are in use. Examples for a diffuse reflector are Al_2O_3 ceramic coatings or white paint covers. Although metals are very good reflectors, their emittance is very low, so that eventually high temperatures would build up in thermal equilibrium. The material studied in this work, second surface metallised FEP, combines the high transmittance of FEP with the high reflectance of metals in the short wavelength region and the high emittance of the FEP space facing surface in the IR region (see figure 1.8). This combination assures very low α/ϵ values and therefore a very good insulation of the spacecraft, which is necessary to keep the fluctuations in the operating temperature low.

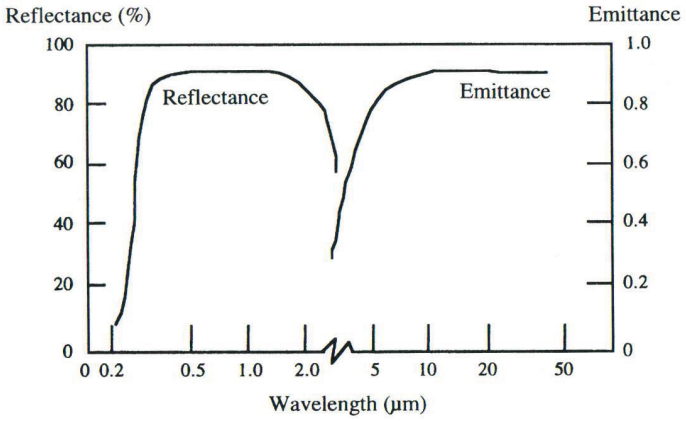

Figure 1.8: Radiation characteristics of silvered FEP thermal control material [17]

1.2 Fluorinated Ethylene Propylene (FEP)

Fluorinated Ethylene Propylene is a copolymer of tetrafuoroethylene (TFE: $CF_2{=}CF_2$) and hexafluoropropylene (HFP: $CF_2{=}CFCF_3$) (chemical name: poly(tetrafluoroethylene-co-hexafluoropropylene). It has essentially the molecular structure of polytetrafuoroethylene (PTFE), but contains -CF_3 branches bonded to the backbone because of the HFP constituent (see figure 1.9). This tertiary carbon is disturbing the crystallinity of PTFE and reducing its melting point from 325°C for PTFE to about 260°C, making FEP a melt processable fully fluorinated polymer. Nevertheless, the advantage of better processability comes also with a reduction in thermal stability, degradation temperature and upper continuous use temperature. The reason therefore lies in the weaker bonding of the -CF_3 side groups, which are preferentially eliminated from the backbone at high temperatures and are also more susceptible to oxidation [18]. Nevertheless, FEP is widely used for its chemical inertness in the chemical industry and for medical applications, as it shows also a good biocompatibility. Material properties as transitions and the content of crystalline phase are strongly depending on the ratio between TFE

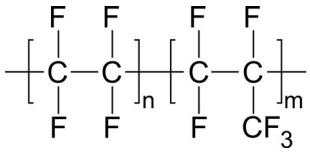

Figure 1.9: Structure of poly(tetrafluoroethylene-co-hexafluoropropylene), FEP

and HFP.
Properties of FEP according to the manufacturer data sheet [19] are as follows:
- Tensile Strength at Break: 21 N/mm^2
- Elongation at Break: 300 %
- Yield Point: 12 MPa
- Elastic Modulus: 480 MPa
- Continous servicing temperature: -240 - 205°C
- Solar transmittance: 96 %
- Coefficient of linear thermal expansion: $9.4 \cdot 10^{-5}$ K^{-1}

1.2.1 Ageing of Teflon® FEP

The ageing of polymer materials is defined as a degradation of its pristine properties (optical, electrical, mechanical or chemical composition), as a result of being exposed to a specific environment. In space, ageing can occur due to exposure to electromagnetic radiation, AO, high temperatures, ionizing radiation and particle bombardment. The combination of more environmental effects can lead to an interaction of ageing processes and result in both, an accelerated or slowed down ageing. This phenomenon is called synergistic effect and is the main reason, why the ageing behaviour of some materials is hard to understand in complex environments.
Physical ageing refers to changes in the morphology by e. g. postcrystallisation and relaxation of residual stresses. These processes are triggered mostly by high temperatures and mechanical stresses. The driving forces can be found in residual stresses induced during the processing steps of the material (e. g. extrusion and irregular cooling conditions during crystallisation). A decrease in molar mass via chemical ageing can also yield to a tendency for re-crystallisation. Chemical ageing is referring to non-reversible reactions, where bonds are broken (chain scissioning), re-established (crosslinking) or a new component is introduced (formation of functional groups). As FEP is a fully fluorinated polymer, it possesses strong C-F bonds with a bonding energy of 486 kJ/mol or 5.04 eV/bond [20]. This bond energy is actually so strong, that atmospheric UV light cannot break the bonds (compare wavelengths in figures 1.6 and 1.5 on page 6) [19]. In space, however, shorter wavelength UV radiation is existent, so that chain scissioning can occur on exposed areas. The penetration depth of radiation is depending on the extent of absorption by the molecules. When FEP is exposed to space conditions, especially wavelengths with attenuation depths in the order of magnitude of the foil thickness can damage the material, via the absorption of the respective photon energies. Due to the high fluences of AO in LEO, also the resistance against AO plays a major role in the space application of FEP. AO reacts with almost all polymers and causes erosion (etching and material mass loss) [21]. Also, FEP is eroding away upon interaction with AO, but with an etch rate of $0.337 \pm 0.005 \cdot 10^{-24}$ cm^3/atom (measured on LDEF with a ram fluence of $9.09 \cdot 10^{21}$ atoms/cm^2) [17]. In fact, when severe degradation of FEP was found on the HST, the assessment of an alternative thermal control material was commissioned. But actually the same materials combination, metallised FEP, was chosen due to its relative inertness and excellent thermo-optical properties. Only a layer of scrim was applied to the adhesive rear part of the foil, so that crack growth would be altered and and curling inhibited [22].

1.2.2 Previous work on the ageing of Teflon® FEP in LEO environment

FEP is an important outer layer thermal control material for missions in LEO and as mentioned above, it was confirmed as the best choice for the outer surface of radiators and MLIs [22]. Nevertheless, FEP was found strongly degraded in the LEO environment showing through thickness cracks in February 1997, after 6.8 years of space exposure.
The first large space exposure test was conducted on board of the Long Duration Exposure Facility from April 1984 till January 1990. A multitude of material samples were exposed to LEO environment to test their ageing behaviour. The results for FEP showed a hazy optical appearance resembling to milky glass and leading to a degradation of thermo-optical properties on the ram-side (facing towards the trajectory of the spacecraft). A clear correlation was found between the discolouration and the assumed AO fluences, so that the phenomena were assumed to be related [23]. An increase of the α/ϵ ratio also leads to a rise in the maximum temperatures reached during thermal cycling, so that recrystallisation of scissioned molecules can be activated, which is in turn leading to a stronger embrittlement.
Calculations show that vacuum ultra violet (VUV) light etches, degrades and heats the surface of FEP where these wavelengths are absorbed (see figure 1.10). The radiation is absorbed in the top layer, where it leads to degradation and etching, simultaneously the absorbed heat is subsequently transferred to lower regions within the foil [20]. In accordance to this, a strongly embrittled surface layer on the solar facing side of space-exposed material was suggested [24] and the occurrence of photo etching due to VUV radiation reported [25]. Erosion can be determined in terms of mass loss and increased surface roughness.
Ionizing radiation is potentially capable of cleaving C-F and C-C bonds, but the rupture C-F bonds is much more likely than the rupture of the weaker C-C bonds [26]. FEP as a fluoropolymer also shows weak intermolecular interactions, so that fluororadicals have long lifetimes of up to three years at room temperature [27]. These radicals can recombine and lead to crosslinking.
For the examination of the mechanical properties normally tensile specimen were punched out of the degraded foils [28] [7]. Recently also relatively small scale (400 µm wide) specimens were tested [29], enabling to test also small pieces of foil samples. Nevertheless, a gradient in the mechanical properties within the foil thickness was not measured before in a direct way. Instead, mostly spectroscopic methods were used [30]. The technique of nano indentation was used to probe cross-sections of aged materials, but did not show significant changes in the hardness over the foil thickness [31]. This can be understood, as the hardness correlates with the strength of the material, but not with its ultimate tensile strength. The latter property is much stronger affected by degradation. An interesting result was obtained by the use of scanning thermal microscopy, where crosslinking due to γ-radiation, chain scission and erosion due to soft X-rays and VUV could be proven [32]. It was also reported, that the combination of AO and VUV exposure are degrading the material by far faster, than both factors separately.

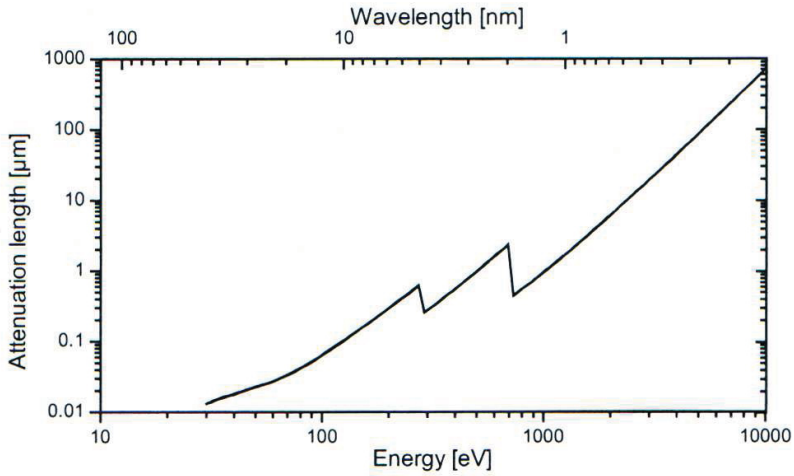

Figure 1.10: Attenuation length of FEP, modelled as C_2F_4 with the density of FEP [7]

2 Methods

A fast and cheap preparation technique is needed to be able to prepare a large number of tensile specimens with dimensions in the range of tens of micrometers. This requires the removal of material with very high precision and high aspect ratios out of FEP foil samples. Further, it is important to find processes which keep the damage during machining and handling as low as possible, so that the results of the mechanical tests are unaffected by the preparation process. To meet the demand for a gentle fabrication, machining close to room temperature (RT) is required. One way of processing FEP is by direct X-ray synchrotron radiation. This photo-etching technique provides the possibility of creating geometries with high aspect ratios [33]. A high intensity light source is needed for this process to achieve fast machining. X-rays are used because FEP is transparent over a wide range of wavelengths, so that visible light cannot be used. By this method high etching rates are only reported in combination with relatively high sample temperatures of 100°C. Another method for preparation of small structures available for FEP is photolithography (for the application of patterns on the material's surface) with subsequent low energy ion (500 eV Ar^+) milling [34]. The step of photolithography requires high temperatures of up to 120°C for the baking of the resist, but ion milling has been carried out by Lee et al. [34] on a cooling stage which lead to well defined structures in the dimension range of *tenths* of micrometers. Unfortunately, as the first preparation step requires high temperatures, this method does not meet the requirement of gentle fabrication either.
In this diploma thesis, techniques of laser ablation, microtomy (for the production of thin sections) and ion milling with a non-photolythographic masking technique were used. Laser ablation would theoretically make the production of flat tensile specimens possible within one machine and minimize the need of handling. On the other side, using the microtome has the advantage of *cutting* the material and therefore not losing any of it by ablation in the step of preparing thin sections. However, microtomy brings also the need of embedding for soft and small samples prior to cutting. Good adherence to the embedding medium is required, which is not easy to accomplish with Teflon ® FEP and also the number of handling steps increases relative to preparation within one machine. For the use of an ion milling system it has to be pointed out that masks with the desired contours need to be available. These masks need to be made of a material, which is eroding with a significantly smaller erosion rate than the investigated material. Copper was used here.
In Leoben, where the experiments were carried out, no suitable laser ablation system was available. Therefore, the development of the production technique concentrated on finding the right set-ups and best procedures leading to specimens with a reproducible high quality with the available tools (microtome and ion milling system).

2.1 Preparation techniques

The preparation of tensile test specimens with dimensions of a few tens of micrometers can be divided into two main steps: the preparation of thin sections (see figure 2.1a)) and the

production of tensile specimens within the thin sections, as depicted in figure 2.1b).

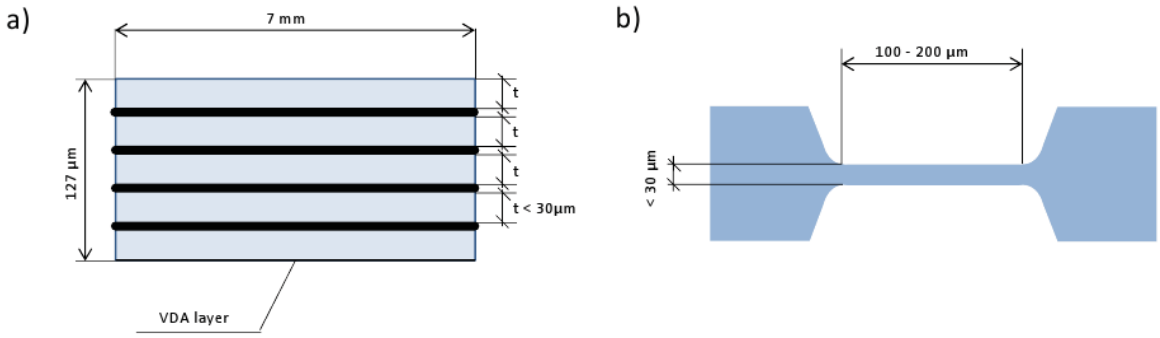

Figure 2.1: Concept of the two-stage specimen processing technique: a) preparing thin sections out of the original foil sample (note: the sketch shows different scales along the axes for better visibility) b) machining the desired dumbbell geometry out of the thin section

Laser ablation and ion milling can be used for both preparation steps, but considering the high aspect ratio of the thin sections, these techniques could reach their limits. Microtomy enables to produce thin sections *only*, but the above mentioned methods can be complemented by it to result in a new sample preparation method.

2.1.1 Thin sectioning with a microtome

Microtomy is a standard method for the preparation of thin sections and flat surfaces of plastics and biological materials. The functional part of a microtome consists of a sample holder and a knife holder with a very precise mechanics making a linear relative motion of these main parts possible. In most designs the knife is fixed and the sample is moved during cutting. The basic operation is as follows:

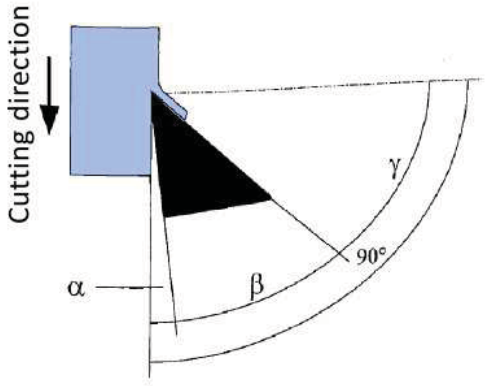

Figure 2.2: Thin sectioning in a microtome in sideview. α: clearence angle, β: knife angle, γ: rake angle, $\alpha + \beta$: sectioning angle [35]

- The sample material is fixed within the microtome and moved into the so called cutting plane. The cutting plane is defined by the linear motion of the sample relative to the knife and the edge of the knife.
- A thin section is cut off from the top layer by moving the sample towards the edge of the knife.
- After each cutting step the sample is withdrawn from the cutting plane to prevent a contact with the knife during moving the sample back above the knife's edge.

- When the sample arrives at its top position a new cutting procedure starts by delivering the sample into the cutting plane.

Sections prepared in a microtome with a thickness of more than 5 µm are referred to as thin whereas thicknesses between 0.2 and 5 µm are called semi-thin sections. Using an ultramicrotome also ultrathin sections with thicknesses smaller than 0.2 µm can be prepared. The thinnest sections are needed for transmission electron microscopy (TEM), where ultrathin sections with less than 100 nm thickness for polymers (and organic substances) and a few tens of nanometres for metals are needed [35].

For the cutting of soft materials rigid embedding and small sectioning areas are essential to minimize the distortion of the thin section due to the cutting forces, called compression. In fact, even the most stiff and hard polymers, like polystyrene PS or poly(methyl methacrylate) PMMA show compressions of up to 30% (see Figure 2.3) [35].
To reduce compression the cutting geometry, especially the clearance angle α and the knife angle β can be reduced. Further also a variation in the cutting speed can lead to better results, as too high speeds result in unnecessarily high cutting forces. To make sectioning of very soft materials (as rubbers) possible, it can be crucial to increase their hardness by cooling them well below their glass transition temperatures [35].

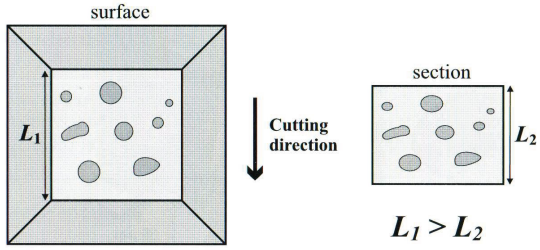

Figure 2.3: Compression of thin sections along the sectioning direction. Left: embedded sample prior to cutting; right: the as-cut thin section. [35]

2.1.2 Embedding of samples

For the preparations of thin sections in the microtome it is necessary to fix the material well in the sample holder for a controlled cut. Some materials can be clamped directly into the microtome, if large enough samples are available. In general, embedding will be necessary to support small and soft specimens. Three media are in general use: epoxy resins and methacrylates [35]. The embedding materials must not react with the examined material and have to have a similar hardness as the examined material. For sections, which are prepared for the use in a scanning electron microscope (SEM) or in a transmission electron microscope (TEM), also the stability of the embedding material in vacuum and under an electron beam have to be considered. Epoxies are the most stable embedding materials in an electron beam, whereas methacrylates are relatively unstable [35]. The polymerisation of cyanoacrylate needs ambient air humidity for polymerisation, so thicker layers of embedding can be reached only by applying the adhesive step-by-step, after the curing of the previous layer.

The Leica RM2255 microtome

For the production of thin sections a Leica RM2255 (see figure 2.4) motorized rotary microtome with an optional cryo-stage for the processing of soft materials was used. This

machine is equipped with an external control panel for setting up the cutting speed in the automatic mode. Section thicknesses in the range from 600 µm down to 0.5 µm can be prepared and automatic cutting velocities are possible from 0.5 to 420 mm/s [36].

Figure 2.4: The Leica RM2255 with its main operational parts [35]

2.1.3 Processing specimens in an argon ion polisher

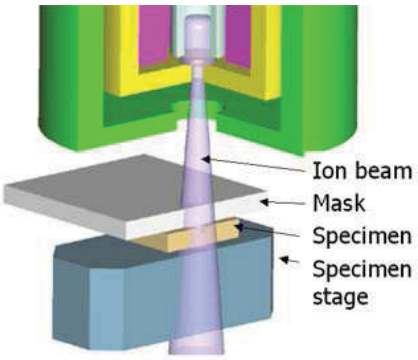

Figure 2.5: The cut away sketch of the ion beam line of the Hitachi E-3500 Ion Milling System [37]

Ion milling is basically a ballistic process of removing material on very small scales. An Argon plasma is produced by a high voltage and Ar^+ ions are extracted by an electric field. After passing an aperture the beam is accelerated towards the sample. A schematic view of such a set-up is depicted in figure 2.5.

The Hitachi E-3500 Ion Milling System

The E-3500 Ion Milling System (see figure 2.6a)) is equipped with a three-electrode ion gun with the Penning system, in which a magnet is incorporated in the electrode block to improve the discharge efficiency. Argon gas is introduced between the anode and cathode

electrodes through the opening in the anode electrode. The plasma generated by applying a voltage of 0 - 4 kV (discharge voltage) between the anode and the cathode electrodes is extracted as an ion beam through the opening in the cathode electrode and accelerated by a voltage of 0 - 6 kV (acceleration voltage) applied between the cathode and acceleration electrodes [37]. The specimen stage unit is designed to be removable from the E-3500 main unit, see figure 2.6b) and c). Like this, the milling position and mask position can easily be adjusted under the separately installed optical microscope, see figure 2.6d) [37].

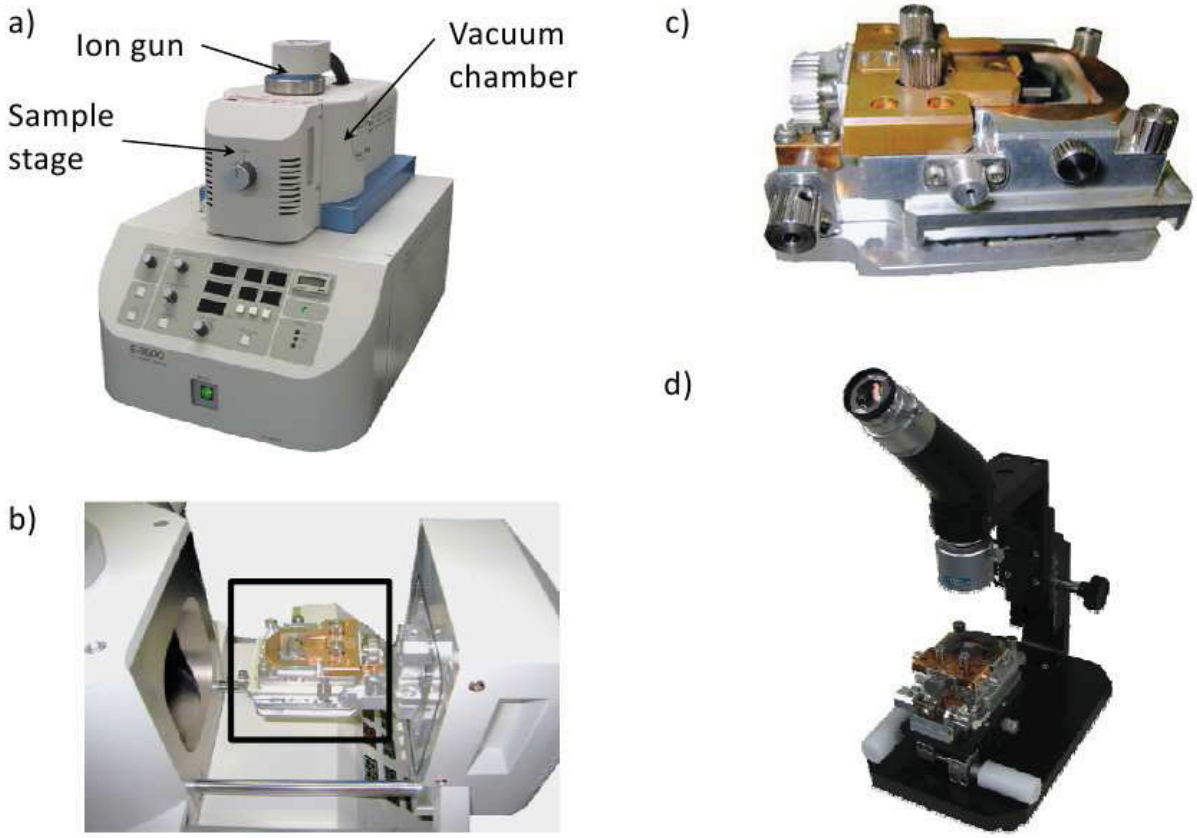

Figure 2.6: a) The Hitachi E-3500 Ion Milling System, b) Open vacuum chamber with sample stage marked by the black frame, c) detail view of the sample stage, d) sample stage fitted under the optical microscope of the system [37]

Masking for thin sectioning

As mentioned above, thin sectioning was also tested in the ion milling system. By tilting the foil specimen with the thin edge towards the ion source and masking areas, which should remain after milling, thin sections were tried to be prepared, see figure 2.7, figure 2.8a) and b). For this processing step the stage rocking was turned on, to avoid milling artefacts called curtaining. This effect comes from the not totally even removal of material and the subsequent self masking of the remained material.

Transfer dumbbell shaped geometries by the masking technique

In a former research project the temperature dependent mechanical properties of copper metallization used in electronic power devices were studied by M. Smolka et al. [38]. There-

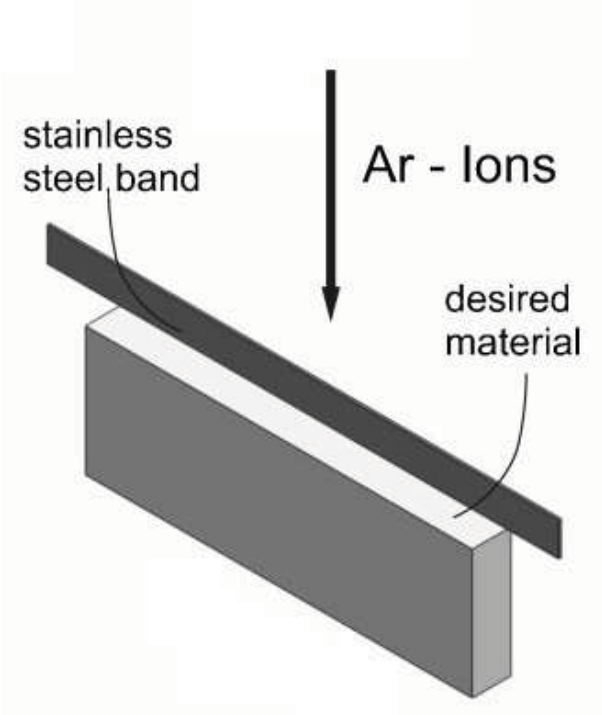

Figure 2.7: Outlines of the aligned thin sections of the sample HST B with the reconstructed average sampling depth (in µm) noted in the head of tensile specimens.

fore electrochemically deposited copper tensile specimen, prepared by photolithography, with a width of 20 µm and a length of 130 µm were used (see figure 2.9). As the dimension and the material of the specimens met the requirements for being utilized as a mask in the ion polisher, a set of copper masks from this earlier study was used.
Due to the geometry of the tensile specimen array it is not possible to use the rocking stage for reducing curtaining. A rotation of the sample stage would lead to bombardment of material under the mask and thus damage the tensile specimens.

2.1.4 Laser ablation

The process of laser ablation is a material removal process by a high intensity laser beam. The energy of the photons is transferred in a primary step into the energy of electronic excitation and in subsequent energy transformation steps resulting in bond breaking and the formation of a plasma plume [39]. Laser wavelengths should lie in regions, where the polymers absorbtance is high to achieve high etch rates and a good coupling of electromagnetic energy into the material. Short laser pulses down to a pulse duration in the order of femto seconds are used to accumulate laser energy for high fluences and to remove layer by layer giving time for the extinction of the plasma created by the previous pulse. The ablation process takes place on such short time scales, that hardly any heat is transferred to the adjacent material. This would be an important advantage of the use of laser ablation for machining small specimens for mechanical testing, as the material would not be affected by machining.

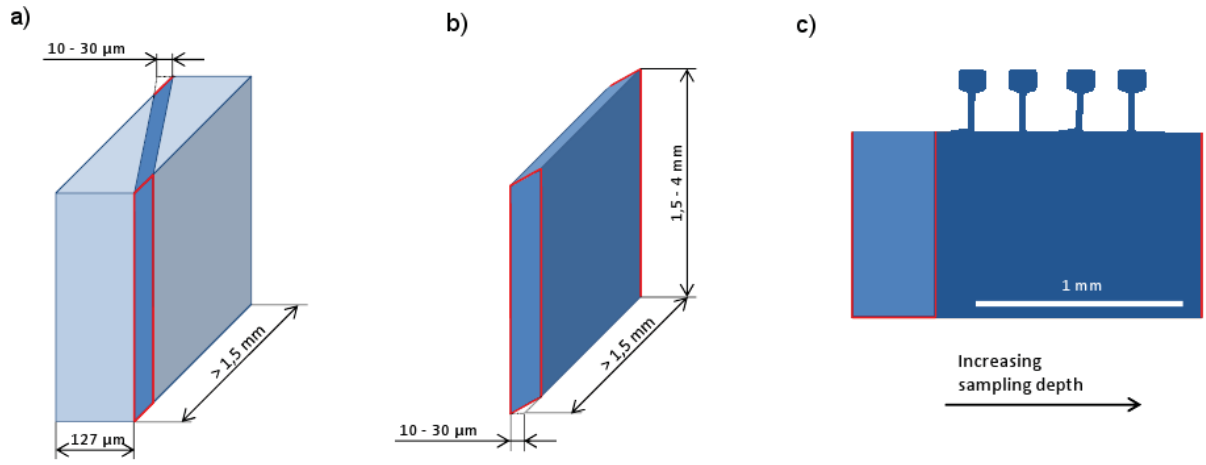

Figure 2.8: Outlines of the aligned thin sections of the sample HST B with the reconstructed average sampling depth (in µm) noted in the head of tensile specimens.

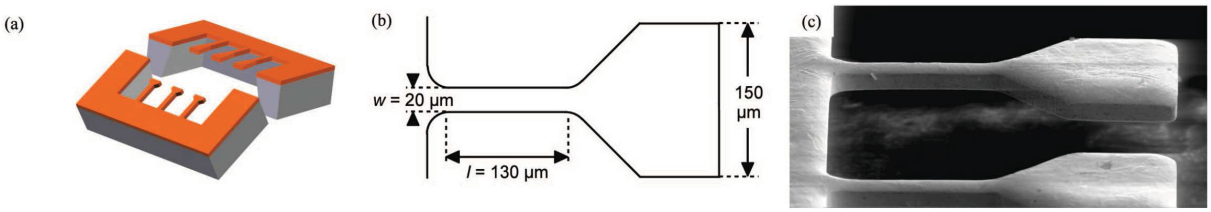

Figure 2.9: a) Schematic of the copper samples bonded onto Si substrate. b) The sample dimensions c) an scanning electron micrograph of the freestanding Cu samples. [38]

2.2 Tensile testing

The tensile tests needed to be carried out on an apparatus, capable of measuring very small forces due to the small cross-section area of the tensile specimen and the soft material of the specimen. For this reason a Kammrath & Weiss fibre tensile test set-up with a measurement range till 2 N and a resolution of 10 µN was used (see figure 2.10). The high resolution in force measurement is attained by detecting the frequency of an oscillating wire. Subtle changes in the load will influence its natural frequency and result in the above mentioned high resolution [40]. The specimens are glued onto a small specimen holder, which can be screwed onto the sample stage. The stage can be moved in all three spatial directions for aligning the tensile specimen. The tensile tests are conducted by a linear movement of the stage along the x-axis. The head of the samples can be gripped with piezo actuated tweezers. For aligning the specimen and documentation purposes, the test is observed via a stereo microscope.
Force and elongation data are recorded and for the calculation of stress-strain curves the specimens are assumed to have rectangular cross-sections.

2.2.1 Thickness measurement of the specimens

To determine the precise geometry of the tensile specimens, a contactless thickness measurement technique is necessary, as specimens are extremely small and fragile. A micrometer gage would exert big compressive stresses onto the material, which has to be avoided.

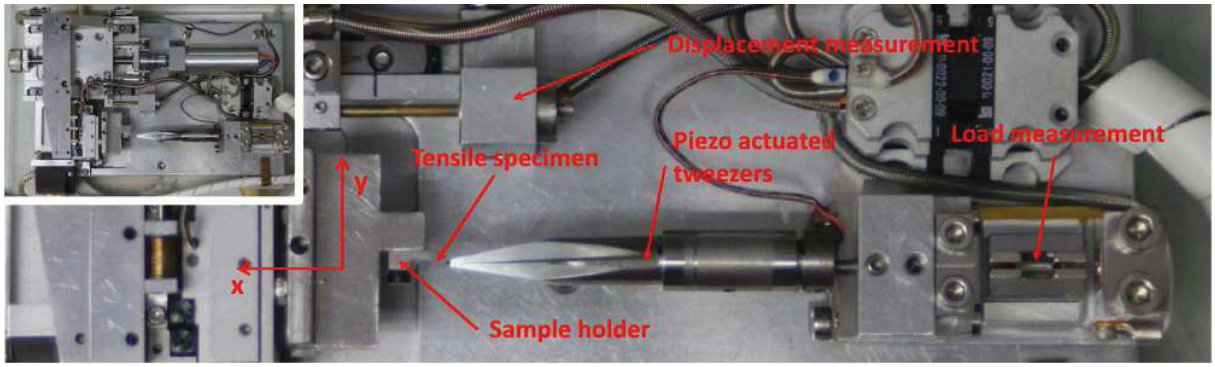

Figure 2.10: Photos of the tensile test module. On the inset the whole apparatus is visible, whereas the major parts of the set-up are labelled in the large figure.

Aligning tensile specimens with the tensile direction parallel to the optical axis of an optical microscope enables measurements of the thickness of the head and the supporting part of the tensile specimen. The use of a scanning electron microscope should be avoided, as the high energy electron beam could cause damage to the sample surface and lead to embrittlement of the samples. Nevertheless, pictures of already tested specimen are well possible in the SEM and provide a very good resolution even without depositing a conductive carbon coating on the samples. Possible other techniques for the measurement of thin foil thicknesses would be: via attenuation of light applying Lambert Beer law (for that FEP shows too little absorptance), via interference with light (possible in UV-Vis-IR spectrometers), or via weighing and measuring the surface area (the density of FEP has to be known). The latter method would be theoretically also possible to apply, but then only an average thickness value could be gained.
The most important thing is to measure the area of the smallest cross-section along the tensile length, to get correct stress values in the stress-strain diagram.

2.3 Spectroscopy

2.3.1 Infrared Spectroscopy

The IR spectrum covers a wide range of wavelengths from the red end of the visible spectrum at 700 µm up to 1 mm. The wavelength region from roughly 2.5 to 50 µm (mid-infrared) is correlating to energies of the vibrational transitions and rotations in molecules, that is why spectroscopy in that wavelength regime is also called vibrational spectroscopy. In the mid-infrared region atoms within a molecule are excited to vibrate, whereas molecules are rotating. Spectra collected in this wavelength region give an insight into the molecular structure of the examined material. Many different vibrational modes can be possible for atoms within a molecular structure, so there is also a corresponding multitude of absorption peaks. By comparing the collected spectrum with references, the molecular substances can be identified [41].

The common way of collecting IR spectra is via the spectral measurement of the transmitted light and is called absorption spectroscopy. But also the spectrum of reflected light can be measured to obtain information about the bindings and molecules in a sample. The attenuated total reflectance (ATR) method makes use of the latter option and enables to

investigate also materials, which are opaque. ATR makes use of the fact, that radiation travelling in a medium of high refractive index, like diamond, is nearly totally reflected at the interface to a medium with lower refractive index at angles larger than the critical angle for total internal reflection. During reflection the light is not contained in the ATR crystal, but rapidly damped just outside of its surface in accordance with an exponential function. This behaviour corresponds to the decay of a wave function at a finite potential barrier in quantum mechanics [42]. The penetration depth of the light beam depends on the wavelength of the light beam, the refractive indices of the sample n_2 and of the ATR crystal n_2 and finally also on the angle of incidence. A sketch of the measuring principle can be found in figure 2.11.

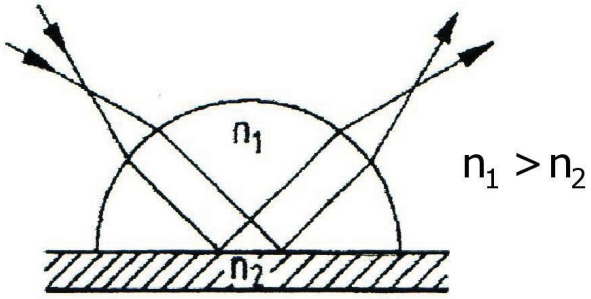

Figure 2.11: ATR measuring principle [43]

As FEP is a co-polymer of PTFE, its absorption bands show a very strong resemblance to the spectrum of FEP and the features of the PTFE spectrum can be found also in FEP. The IR spectrum of PTFE shows a strong and wide absorption band near 1200 cm $^{-1}$, which comes from CF_2 stretching and consists of three peaks at 1240, 1215 and 1150 cm^{-1}. Other major bands can be assigned to to the CF bending modes and are located at 641, 554 and 515 cm^{-1}. Contrary to Raman spectroscopy skeletal C-C stretching is observed only as a weak and complex band. A specific band produced by the hexafluoropropylene moiety of FEP can be found at 982 cm^{-1} [44].
Measurements were performed on a Perkin Elmer Spectrum GX IR spectrophotometer with an attenuated total reflectance (ATR) diamond crystal, which enables measurements in the wavenumber range of 4000 to 370 cm^{-1}.

2.3.2 Raman Spectroscopy

Raman spectroscopy is closely related to IR spectroscopy, as both methods are probing molecular vibrations, but the interaction of the monochromatic electromagnetic radiation of the probing laser and the examined material is based on another effect, the Raman scattering. Only a very small portion of the incoming light ν_0 is scattered inelastically (yield is small) and shifting therefore its frequency ν_0 to ν_R. The spectrum of the inelastically scattered light shows bands with wavelength shifts corresponding to the vibrational modes of the molecules. Shifts to lower frequencies than ν_0 are called Stokes lines, shifts to higher frequencies anti-Stokes lines. The formation of the Raman spectrum can be understood as the difference in energy $\Delta E = h \cdot (\nu_0 - \nu_R)$ to change the vibrational state of the molecule. If the exciting energy $h\nu_0$ is high enough to excite an electron into a higher electronic state, the Raman scattering can be concealed by fluorescence, see figure 2.12a). During Stokes scattering the vibrational energy of the molecule is increased, yielding ν_R being lower than

ν_0, see figure 2.12b). Contrary anti-Stokes scattering means a reduction of vibrational energy and ν_R being greater than ν_0, see figure 2.12c).

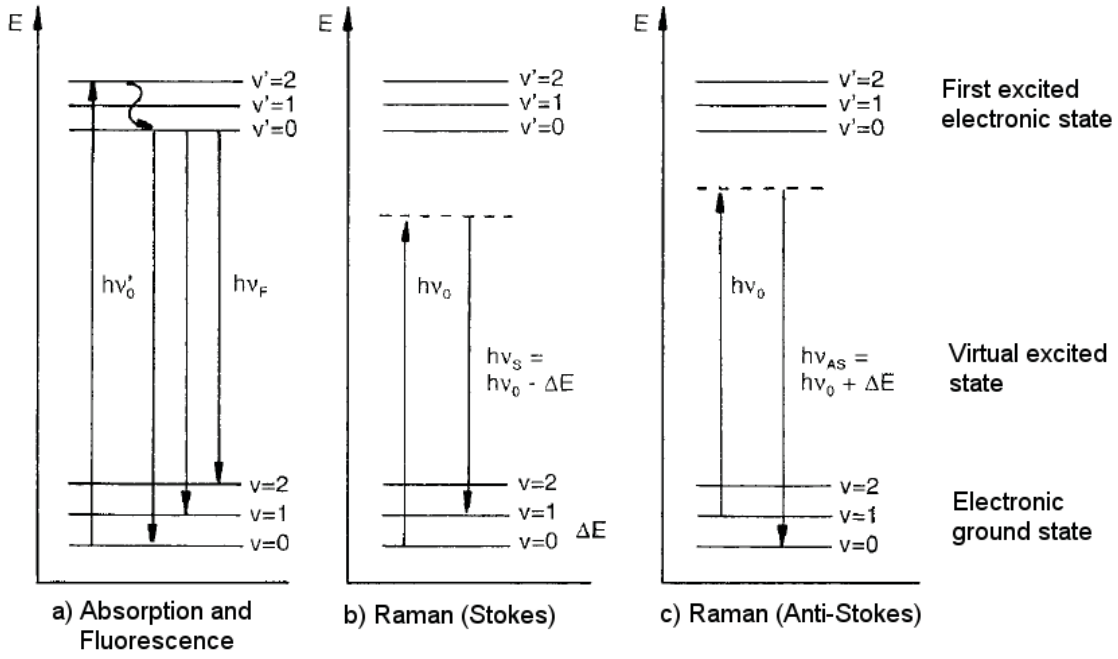

Figure 2.12: Interaction of monochromatic light with molecules (ν and $\nu\prime$ vibrational quantum number of vibrational modes in the electronic ground state and excited state, ν_0 and $\nu_0\prime$ excitation frequencies, ν_F fluorescence frequencies, $\nu_0 - \nu_{AS}$ anti-Stokes Raman shift) [45]

The Raman spectrum of PTFE shows the most intense band at 734 cm^{-1} and this is assigned to the skeletal C-C stretching band. Further, three weak CF_2 stretching bands between 1400 and 1200 cm^{-1} and two bands at 386 and 293 cm^{-1} can be measured, which are assigned to CF_2 rocking vibration [44].

As in IR spectroscopy, also the Raman spectrum of FEP is very similar to the one of PTFE and shows only a few peaks with wide spectral windows of featureless background. Because it is a totally fluorinated polymer, the spectral bands occur at different wavenumber shifts as the ones of important other materials [46]. The latter fact would make a detection of new bonds relatively easy.

Measurements were performed on a Horiba Jobin Yvon Raman Microscope with an optical table and a red laser (632 nm). The lateral and vertical resolutions of the instrument are 1 µm and 2 µm respectively. Spectral data can be collected with a resolution of 0.5 cm^{-1} and for the actual measurements gathered from a depth of 8 µm under the surface of the thins sections.

3 Development of the tensile specimen preparation technique

For the resolution of a possible gradient in mechanical properties within the thickness of space exposed Teflon® FEP, dumbbell shaped tensile specimens need to be prepared with a thickness between 10 and 30 µm. Lower thicknesses would increase the spatial resolution of the obtained information. Contrary, with smaller specimen sizes the effect of irregularities in the sample geometry (which are depending on the machining technique) on the tensile behaviour would increase. Finally, also the limited sensitivity of force measurement during tensile testing can inhibit the use of very small cross-sections. A reproducible preparation procedure could be found with the use of machining steps in a microtome and an Ar^+ ion milling system. Focussed ion beam (FIB) and laser ablation techniques were assessed in single tests.

3.1 Progress towards the final preparation technique

For the development of a machining technique leading to reproducible specimen geometries pristine Teflon ® FEP/VDA foils were available. First plans foresaw the whole sample preparation in an ion milling system, meaning first the preparation of a thin section and after that turning and masking with copper masks of the desired tensile specimen shape. As the first step at producing a thin section could not be accomplished within the ion polisher, the use of a microtome was introduced into the development procedure to prepare thin sections. Using the microtome also meant that the foil samples had to be embedded. This meant not only extra handling steps, but also a good embedding technique had to be found to enable good sectioning results.
The preparation of the dumbbell shaped specimen geometry was tested first with a 7.5 µm Upilex-S®[i] foil. Hereby, the possibility of transfering the geometry of the tensile specimen onto thin sections was assessed, without the need of preparing thin sections out of the FEP foil. For masking in the ion milling system, existing copper tensile specimen with the desired shape were used. The copper masks were developed for the research of the behaviour of copper connects in the microelectronics industry and were prepared by photolithography. After the proof of principle by preparing the first successful tensile tests on specimens machined out of pristine FEP foil samples, finally aged samples (especially from the solar facing side) of the HST SADA MLI were subject of testing.

3.1.1 Cleaning the foil samples

Prior to sample preparation, a sample of pristine foil was cleaned by isopropyl alcohol, which lead to white translucent spots. These marks did not fade away even after storing the sample for a month in a desiccator. Rinsing of foil samples with deionized water and ethanol

[i] Upilex is a registered trademark of UBE INDUSTRIES, LTD.

did not show the mentioned effect, but still cleaning was avoided in the later developed procedure. Instead the focus was on not contaminating the samples, thus during handling a lot of care was taken in respect to the cleanliness. Avoiding cleaning also means a reduction in handling steps and therefore an overall improvement of the results.

3.1.2 Embedding of foil samples

For the first sectioning tests, Teflon® FEP/VDA foil samples were embedded in epoxy resin (EpoFix resin and hardener from Struers). Therefore foil samples with a surface area in the range of the aged HST foil samples (~7×4 mm) were cut out from the available pristine FEP material with a razor blade and placed on the bottom of a flexible polymer mold for embedding. To inhibit the floating of the light, small and hydrophobic foil it was backed up by a M6 metal nut with a plastic clamp as a spacer in-between. Although most of the so prepared samples could be processed in the microtome, a debonding after the first few thin sections occurred. Another disadvantage proved to be the limited aligning possibilities of the foil sample during casting. Sometimes samples were unevenly embedded or air bubbles trapped just behind the foil inhibited their further use. To avoid these problems another embedding possibility was searched for.
Using UHU®[ii] Sekundenkleber blitzschnell cyanoacrylate adhesive for sticking the foil sample with the metallized surface onto a supporting polyamide (PA) block proved to yield to better results, although debonding during sectioning and curling during curing of the adhesive were observed with some samples. The reason for the latter problem could not be found, although a too thick application of the adhesive or contamination of the surfaces by moisture or grease were suspected.

3.1.3 Preparing thin sections with the microtome

During the first tests with the microtome, different thin section thicknesses were prepared. With the aim of good depth resolution a thin section would have the advantage of enabling the testing of mechanical properties within thinner layers of the material. In contrast to that, the tensile test results gathered with thinner specimens were being expected to be increasingly influenced by the imperfect surface quality, which is given by the used fabrication techniques (microtomy and ion polishing). Thin sections of less than 15 µm could not be prepared without immediate tight curling of the sections, so the value of 15 µm was accepted as a lowest possible thickness. As the copper masks for the preparation of the dumbbell shaped specimen were available in widths of 10, 20 and 30 µm (measured at the test length), the next biggest mask of 20 µm was chosen. To get specimens with a square-shaped cross-section area along the test length, also the thin sections were chosen to be 20 µm thick.
A knife with tungsten-carbide edge was utilized with a clearance angle of ~5°.

During a test run utilizing the cooling stage of the microtome no useful thin sections could be produced due to the debonding of the foil samples from the epoxy embedding. Thus, no cooling was used during microtomy.

[ii] UHU is a registered trademark of UHU GmbH & Co KG

3.1.4 Transferring the dumbbell shape onto thin sections

First tests in the ion milling system were conducted with UPILEX-S foils to assess the possibility of transferring the dumbbell shaped specimen geometry from copper tensile specimens (with the same shape and size as the desired geometry). When the right set-up of ion beam current and acceleration voltage were found to reproduce the shape of the copper mask, the first tests with FEP thin sections followed. As the copper mask was placed with its silicon supportive layer on top of the thin section (to avoid the damage of the copper specimen), there was always a gap - of the thickness of the silicon layer - between the mask and the thin section. This technique resulted mostly in acceptable tensile geometries, but reproducibility was not good. Actually, the formation of thin layer was found to deposit on the top layer of the first prepared specimens prepared in this way, see figure 3.1. The EDX analysis of this material showed the existence of iron and copper, which is thought to be eroding from the mask and the sample holder during processing the thin sections in the ion polisher (EDX set-up: aperture: 60 µm, AV: 12 kV, 60 Degrees tilted, tensile specimens point downwards, working distance: 14mm).

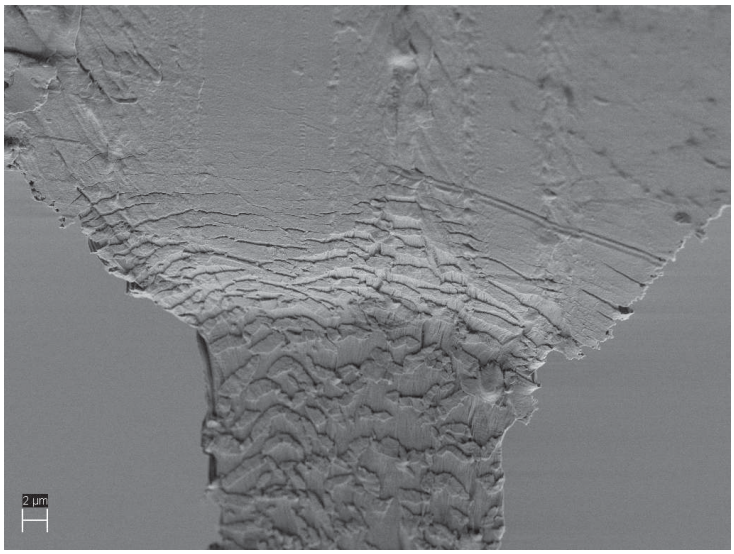

Figure 3.1: SEM micrograph of a sample prepared with a small gap between the mask and the thin section, after tensile testing. The cracking of a surface layer is visible at elongated areas.

3.1.5 Surface structure and possible damages

Although specimens with well defined and regular geometries can be machined, the surface of tensile specimen is not free of defects. The edges are eroded by ion milling and show a structure, as it is visible in figure 3.2a). But the influence of this structure on the tensile tests should be relatively small, when testing a ductile material like FEP at low strain rates. Grooves originating from the thin sectioning process on the upper and lower faces of the specimens are also of a minor concern, if they are oriented parallel to the tensile length. Residual stresses originating from sectioning might interfere with the applied load during the first part of tensile testing, resulting in a reduction of the measured yield strength, but this

effect is considered as having also a low impact on the measured ultimate tensile properties. In contrast, all damage due to ions passing under the mask have to be avoided, for attaining a good tensile specimen. Damage due to ion irradiation of the tensile specimen surface can be seen in figure 3.2b). To avoid ions penetrating under the mask, it was placed with the copper side directly on top of the thin section in the later evolved final sample preparation technique.

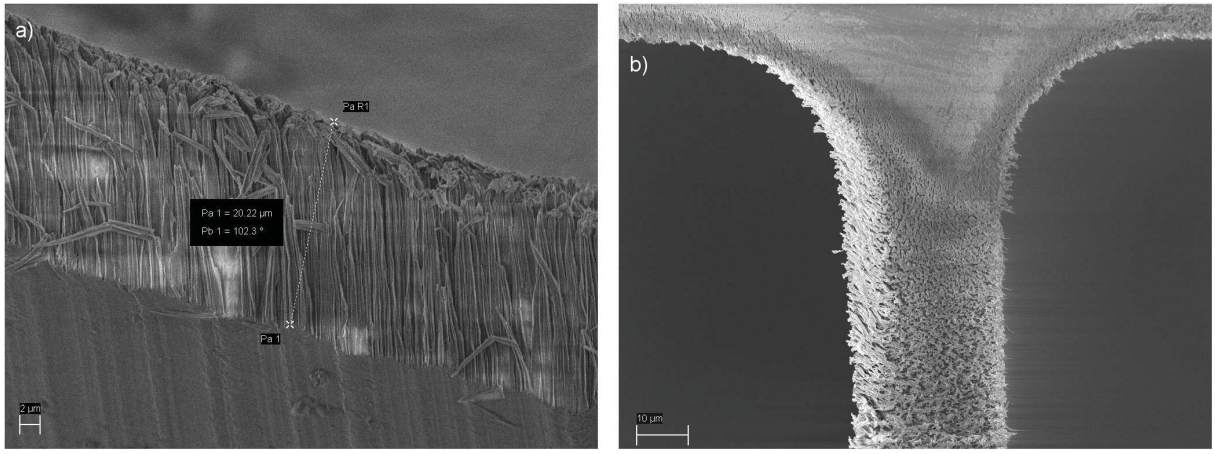

Figure 3.2: SEM micrographs of thin sections machined with a small gap between the mask and the thin section (after tensile testing). a): edge of the ion milled thin section. b): damage due to ions passing under the copper mask.

3.2 Final sample preparation technique

The workflow of the developed sample preparation, documentation and tensile testing are presented in this section in a step-by-step listed way. In general it can be said, that it is essential to use well maintained tools for getting good results. Especially the importance of the right type of tweezers for specimen handling should be pointed out. Easiest and best handling experience of the foil and the thin sections could be achieved by using straight metal tweezers with super thin tips and without inside serrations (Dumont Style 5). The handling of other and especially harder parts should be carried out with another pair of tweezers to prevent small damages on the tip while gripping. The working places and tools have to be kept as clean as possible to prevent contamination of sample surfaces. For that use surgical gloves and clean especially the parts of the used tools, which will get into direct contact with the samples. Spreading aluminium foil over the working place assures a surface free of grease and dust.

1. Take pictures of the complete foil 'as received' under an optical microscope
2. Embedding the sample

    - If needed, the sample has to be trimmed to assure a good result during thin sectioning in the microtome. As a rule of the thumb the specimen should not exceed 7 mm in width and hight.
    - Prepare a 2 - 3 cm high polymer block - made of polyamide - and a slightly bigger top surface area than the sample to be embed. Grind the top surface with 800

grade abrasive paper so it gets leveled out, but also shows a slight roughness to ease the distribution of cyanoacrylate adhesive.

- Place a small droplet of cyanoacrylate adhesive on the prepared polymer block top surface and distribute the glue to get a thin layer of adhesive. Place the sample in the middle of the wetted area and wait till the glue hardens. It is possible to press the sample carefully onto the block, but then it is essential, that no adhesive gets between the tool (polished metal surface of a razor blade e.g.), otherwise the sample might get stuck to the tool.
- After the sample is well adhered, the edge of the polymer block surface which is not covered by the sample should be filled up with more cyanoacrylate adhesive step by step to support also the edges of the sample. To be able to dispense very small amounts of glue on the edge of the sample, a needle can be used to transfer adhesive from a bigger droplet.
- Let the glue harden for at least 24 hours in ambient atmosphere. Cyanoacrylate needs air humidity for polymerization. The thinner the subsequently applied layers of glue, the faster the polymerization process.
- It is basically also possible to embed samples in epoxy resin, but for FEP foils this way of fixation lead to a lower yield in successful thin sections due to de-bonding of the sample while cutting.

3. Take pictures of the embedded sample

4. Thin sectioning in a microtome
    - Use a massive steel blade with a cutting edge made out of cemented carbide. Set the clearance angle to about 5° (for definition of the clearance angle see figure 2.2 on page 15).
    - Clamp the embedded sample into the microtome and tilt the sample surface in a very small angle relative to the cutting plane (nearly parallel) in order to make sure that the part of the sample, which is reached by the blade at last is closer to the cutting tool. This set-up proved to result in the smallest amount of samples breaking out of the embedding. The cutting planes should be aligned in a similar way, as depicted in figure 4.2.
    - Set-up the desired thickness (20 µm) of the thin sections by adjusting the delivery step size to that value.
    - Depending on the hardness of the material and the thickness of the thin sections the right cutting speed has to be found. Slow cutting speeds can result in uneven sections and too high speeds exert unnecessarily high shear stresses onto the sample, resulting in stronger curling of the sections and in the worst case in the de-bonding of the sample out of its embedding.
    - Thin sections should be collected immediately after each cutting step and put in between a pair of cover glasses. It is possible to put more thin sections between the same pair of cover glasses, but it is most important, that the sequence of the sections is re-traceable. For easier reconstruction of the sampling depth, take care of positioning the sections oriented the same way relative to their original position in the foil sample.

- For transportation and storage of the thin sections, the pair of cover glasses can be backed up by another pair of the same coverslips, which then can be hold together by wrapping it in aluminium foil or holding the outer layer together by adhesive tape. This measure ensures that the first pair of cover glasses are kept clean and the samples in between are fixed at their original positions. Later it is possible to take micrographs in an optical microscope directly in between the first pair of cover glasses without the need of touching the thin sections.

5. Take pictures of the thin sections.
   - To ease the reconstruction of the original foil out of the pictures, align the fine grooves from microtomy (showing the cutting direction) parallel to one of the edges of the picture.
   - Also take care, that the orientation of the sections is the same by trying to overlap consecutive sections. If the grooves of the thin sections are oriented the same way, only a rotation by 180° and/or mirroring should be necessary.
6. Reconstruct the position of the thin sections within the original foil sample and chose relevant positions, where the tensile specimen should be machined out of.
   - Use a software tool (Bézier-curves in Inkscape e.g.) to trace the edges of the thin sections, each with a different colour referring back to them. Pay attention, that the sections have to be aligned in the same way relative to their original position within the foil sample.
   - Stack the outlines of the thin sections on top of each other in a way, that originally overlapping edges come to rest on top of one another.
   - By tracing back the edges, which were originally on the top surface of the foil and assuming a uniform thickness of the thin sections as set-up during microtomy, the sampling depth of different positions within a thin section can be reconstructed. Count the number of layers above the position of interest and multiply it with the sectioning thickness. Add the averaged thickness of the very top layer, which will in general not be the full thickness of the thin section.
   - Mark the positions of interest on the micrographs of the thin sections and see how the dumbbell shaped specimen would fit in the best by superimposing its contours with the thin section.
7. Fix thin sections for easier handling in the sample holder of the ion milling system with conductive carbon cement onto a small piece of silicon wafer. Use as little cement as possible and do not wet the part of the sample, where the tensile specimens should be machined out of.
8. Aligning the tensile specimens of the copper mask parallel to the cutting direction and at the desired position.
   - A sample holder with two clamps should be used.
   - Fix the piece of silicon wafer with the attached thin section with one clamp.
   - Place the copper mask directly on top of the thin section (copper side touching the thin section and silicon base pointing up) close to the desired sampling position.

- Move the copper mask carefully into its desired position using a pair of tweezers with super sharp tips. Use the second clamp to hold the copper mask in place when the right position is found. This step should be carried out under an optical microscope without image rotation to prevent wrong movements during positioning and to reduce handling time and damage to the surface of the thin section (see figure 3.3).

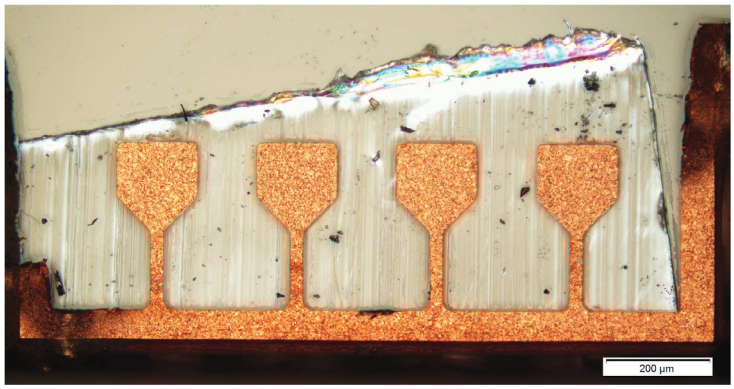

Figure 3.3: Optical micrograph of the copper mask lying directly on top of the thin section and aligned parallel to the cutting direction (visible via the groves). In the background the highly reflective and smoth surface of the supportive silicon wafer piece is visible.

- When the alignment is finished, position the ion milling sample holder into the adjustable sample holder stage.

9. Align the position of the ion beam centre about 100 µm away from the row of tensile specimen heads. This should assure a uniform milling over the whole array of specimens.

10. Ion milling
    - Turn on the high voltage of the ion milling system for a certain time in advance to assure a constant and stable ion beam.
    - Build in the sample stage and start milling with the following set-up when using the Hitachi E-3500 Ion Milling System for machining FEP thin sections:
      acceleration voltage: 1.7 kV
      discharge voltage: 3.6 kV
      ion beam current: ~60 µA (Regulate the argon gas flow to achieve this value.)
      stage control: off (no stage reciprocations)
      milling time: 8 minutes
    - For documentation and possibly necessary re-adjustment of the Ar gas flow check the ion beam current during milling (at 6, 3 and 1 minute remaining milling time).

11. Take photos of the array of specimens and measure the smallest width and the test length of the tensile specimens. Figure 3.4 shows the sample stage directly after ion milling.

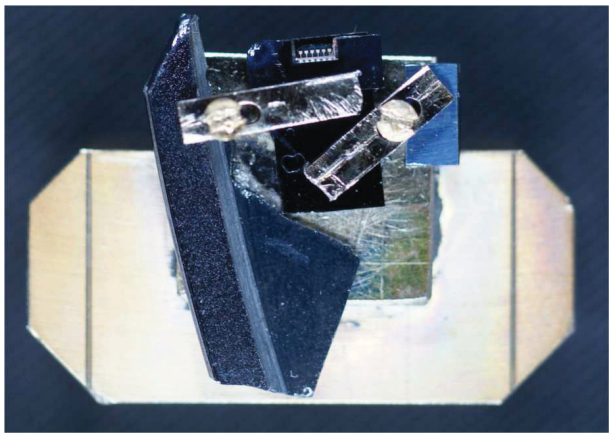

Figure 3.4: Sample stage with built in mask but already eroded thin section around the masked areas

12. Remove thin section from silicon wafer and glue it carefully onto the specimen holder for the tensile test set-up. Special caution has to be taken here to the strong capillary forces, which can pull the thin section into the wet adhesive. To avoid this scenario the thin section has to be held till the viscosity of the glue starts to increase remarkably, shortly before bonding.

13. Measure the thickness of the tensile specimen at the head of the specimen in the optical microscope by tilting the tensile specimen test length parallel to the optical axis.

14. Perform tensile tests
    - Set-up tensile testing facility (Kammrath & Weiss fibre tensile test set-up with piezo actuated tweezers) and calibrate force measurement. Calibration of the elongation measurement can be checked later via photos of the test.
    - Use an optical (stereo-) microscope and a camera to be able to document the progress of the test.
    - Build in the sample holder with attached tensile specimens and align the axis of the specimens parallel to the tensile direction.
    - Position the first tensile specimen head just in front of the tip of the tweezers. The alignment in z-direction can be achieved by finding the same focal plane as for the tip of the tweezers.
    - Use the highest magnification of the optical microscope, where specimen elongated by up to 800% still would fit in the image.
    - Open the tweezers and move the head of the specimen in between.
    - Take care while closing the tweezers, as the tip might be moving away from its original position, requiring a tracking of the specimen via the sample stage. This measure helps to reduce the pre-load before starting the actual tensile test.
    - Perform tensile testing and take regularly pictures of the process till the specimen breaks.

- Move sample stage into a safe distance from the tip of the tweezers (up in the z-direction) and open the tweezers to release the head of the specimen.
- To actually remove the head of the specimen from the tweezers, use an eyelash gripped with a pair of manual tweezers to sweep it away.

15. Measure the thickness at the 'bottom' of the tested samples in a similar way as when measuring the thickness of the head of the specimen.
16. Process the collected elongation, force and dimensions data to obtain the measured stress-strain-curve.

3.3 An alternative machining possibility: laser ablation

For the test of laser ablation methods for the production of thin sections on FEP foil, a sample was machined by the research group of laser micromachining of materials at the University of Salamanca, Spain. A titanium-sapphire laser with two amplifier stages emitting 120 fs pulses centred at 795 nm and a maximum energy of 1 mJ (at 1 kHz) or 50 mJ (at 10 Hz) was used. Instead of the initially desired machining of a thin section only a 500µm long and 160µm deep furrow could be prepared, see figure 3.5. As the laser beam needed to be focused for machining, the cone of light in front of the focal plane was started to get attenuated by the upper edge of the machined furrow. So, basically the production of tensile specimen by laser ablation seems to be possible, but a lot of improvement would be needed to be able to produce similar samples, as the ones prepared via microtomy and ion polishing.

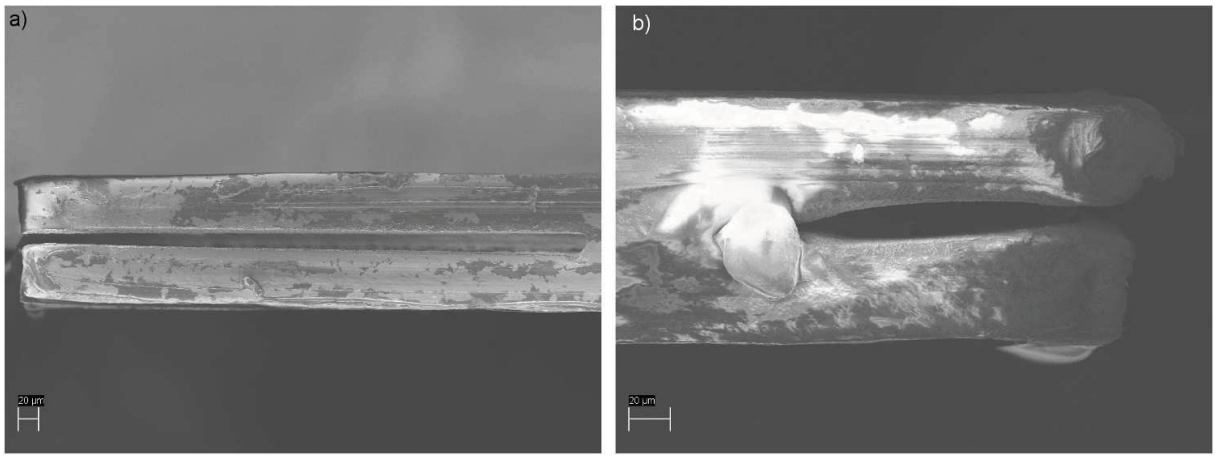

Figure 3.5: SEM micrograph showing a laser ablated furrow at the edge of a 127µm thick FEP/VDA sample. a) More than 500µm long laser ablated region, view from side, where the sample was machined from. b) View direction perpendicular relative to a); the ablated furrow reached a depth of 160µm.

3.4 Attempts of producing thin sections with the masking technique in the ion polisher

3.4.1 Masking with a steel foil

In the beginning of this work it was aimed to prepare the samples only with the ion polisher and two different masks. Firstly a thin section with 10 - 30 µm thickness should be machined out of the 127 µm thick foil with a certain inclination relative to the original surfaces, see figure 2.8a) on page 20. Doing so, material from different depths could be probed within one thin section. A parameter study was started to find the the best milling set-up, giving the smoothest and largest thin section areas. The distance between the masking foil and the sample's edge was reduced and also different stage rock speeds were tested. Nevertheless, no thin section could be produced by this technique.

3.4.2 Masking with the edge of a titanium mask

The set-up of this ion milling machining test looked very similar to the situation depicted in figure 2.5 on page 17. Seen from a direction parallel to the ion beam, the foil was installed edgewise and part of this upwards facing edge was covered by a titanium mask. For producing thin sections it would have been necessary to turn the sample by 180°, to remove also material from the other side of the the same upwards facing edge. In other words, this method would etch away material first on one side of the desired thin section only. However, this method also was not successful and structures similar to those produced by the masking with a stainless steel band were achieved (see figure 3.6).

Figure 3.6: SEM micrographs of two specimens after the attempt of producing thin sections in the ion polisher; left picture: masking with a stainless steel band, right picture: masking with a titanium mask.

3.4.3 Machining FEP with a Focused Ion Beam

When it was evident, that the machining of thin sections could not be achieved by using masking available masking techniques, sample preparation in the FIB was tested. Although it was clear that for the final sample preparation technique the FIB will not be used, milling with Gallium ions was tested on a small surface area of about 10 x 5 µm.

Further, also the Gas Injection System (GIS), installed in the FIB, was tested and an area of 1 x 1 µm covered by tungsten. The idea here was to deposit the mask needed for ion polishing directly on the foil sample, although this type of preparation would have had the negative side, that the masking material would have remained directly on top of the specimen. Both of the tests were successful, but machining in the FIB did not qualify for the final sample preparation technique due to the damaging potential of the Gallium ions and the slow processing speeds.

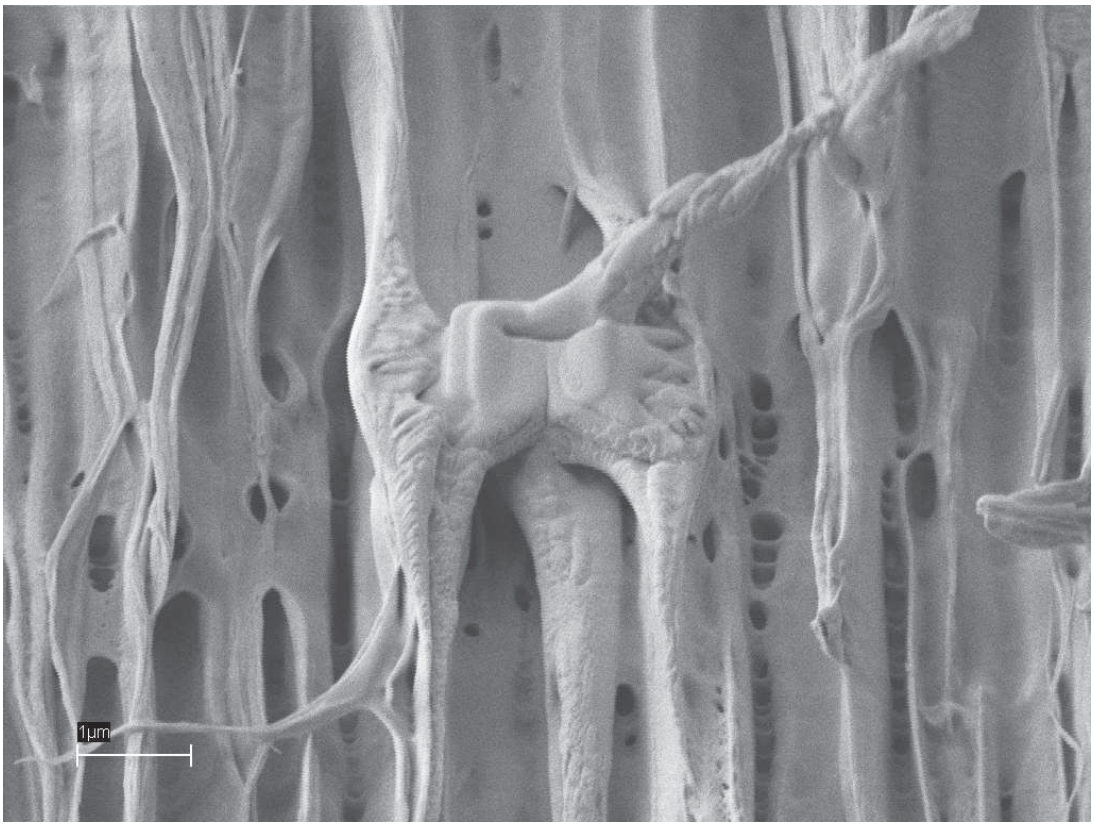

Figure 3.7: SEM picture of a 1 µm x 1 µm tungsten island deposited on FEP, the surface roughness is due to ion polishing, with the ion trajectory in the image plane parallel to the short edge of the figure.

4 Experiments and Discussion

Tensile specimens in the size range of a few tens of micrometers are needed to resolve the difference in mechanical properties between a potentially embrittled layer within the thickness of aged FEP foil. Firstly, the main effort was put into the production of tensile specimen, but soon after the first successful specimens were produced, testing needed to be focussed on. The Kammrath & Weiss fibre tensile set-up was mainly chosen for its high resolution in force measurement. The same test set-up was tried, as the one utilized by Smolka et al. for the very same copper tensile specimen, which were used as masks in this work. But due to the much lower stiffness of polymers, the head of pre-test-run specimens always slipped out of a silicon mold, made for fixing the head of the copper samples, see figure 4.1. To resolve this problem an active gripping tool was needed.

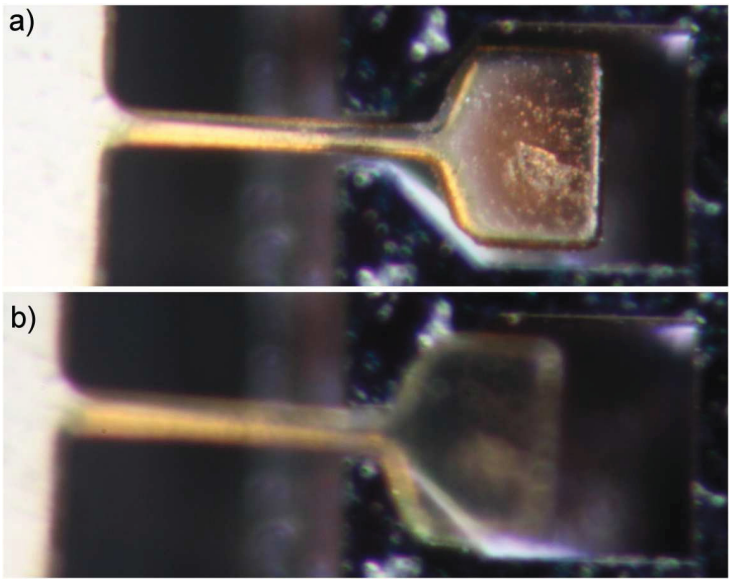

Figure 4.1: A specimen of the pre-test series tested in the Kammrath & Weiss tensile test apparatus with a silicon sample head gripper, wich is used normally for copper specimens. a) before the load was applied b) shortly before the specimen head slipped out of the gripper.

4.1 Optimization of the tensile test set-up

The test set-up for testing copper specimens could not be used due to slipping of the sample head, as mentioned above. The main changes in set-up were the utilization of piezo actuated tweezers to grip the sample heads and the bonding of the samples to the sample holder by cyanoacrylate adhesive, instead of clamping the samples. When using the piezo

actuated tweezers, the sample heads were deforming so much, that material was pressed out from between the tweezers. As a matter of fact it was not possible to control or measure the gripping force. The tweezers were always closed totally, to treat all samples the same way and avoid a slipping of specimen heads. After the right set-up for ion milling was assessed, nine foil samples of aged material from different positions of the HST SADA MLI (HST A - HST I) were subject to prove the possibilities provided by the developed preparation technique and micro-mechanical testing (see figure 1.3 on page 4).
To attain reproducible and comparable results, tests were carried out in an air-conditioned room (SEM laboratory) at temperatures of about 22°C and a relative humidity of 30% . Also, the testing speed was kept constantly at 0.5 µm/s, which equals a strain rate of $3 \cdot 10^{-3}$ s^{-1}. The specimen length to width ratio was given by the thickness of the thin sections and the geometry of the used masks, showing a nominal value of 6.5 : 1. The individual dimensions as thickness, length and width were measured prior to testing under an optical microscope. Reproducible tensile tests could be performed only with specimen with tensile directions parallel to the cutting direction, so after the evaluation phase of this work, only such specimens were used.

4.2 Reconstruction of the original foil sample - finding the sampling depth within thin sections

For finding the position of the tensile specimens, a good documentation of the thin sections during the sample preparation process is necessary. In this work the sampling depth was determined by a graphical method, where the edges of thin sections were superimposed again in the same way, as in the original foil sample (see figure 4.2). The contours of thin sections were traced with a software tool, to create closed curves with the outline of the samples within the thin sections. The position of edges, which were etched away during ion milling could be found by matching back to the state before ion polishing. For the actual reconstruction, a uniform thickness of the thin sections was assumed. In a first step those edges of the stacked outlines needed to be identified, which originally lay on the top surface of the foil sample. Above the position of interest, the number of full thickness layers were counted and multiplied with the thickness of the sections. After this, the averaged thickness of the very top layer (which was in general not a full thickness section) was added to obtain the sampling depth measured from the sample surface.
Like this the average sampling depth at the middle of each tensile length was found. Figure 4.3 shows the stack of outlines, which were used to find the sampling depth in HST A sample. The obtained depth information is written in the respective head of the specimen. Each colour is matched to a thin section, namely: HST A-M1, HST A-M2, HST A-M3, HST A-4, HST A-M5, HST A-M6, HST A-M7, HST A-M8, HST A-M9, HST A-M10.

4.3 Investigation of aged FEP retrieved from HST

The investigation of aged FEP samples retrieved from the HST and taken from the SADA MLI was the driving force for the development of the stated specimen production technique.

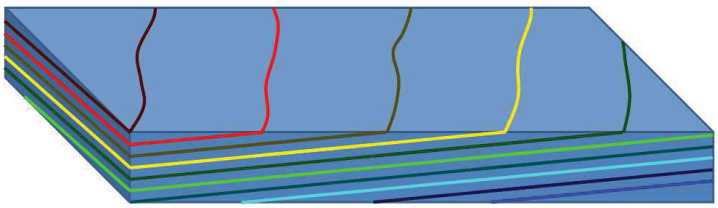

Figure 4.2: Three dimensional sketch of a reconstructed sample. The coloured lines are marking the edge of the thin sections.

4.3.1 Tensile tests

The measured force and elongation data was processed with the thickness measurements in an optical microscope to obtain stress-strain curves of the samples. The test speed was set rather low to 0.5 µm/s, which equals a strain rate of $3 \cdot 10^{-3}$ s^{-1}. Comparing the results of HST A, HST B and HST D it can be seen, that the mechanical properties degrade towards the direct solar facing position of HST D. The latter foil sample was the only one, where samples close to the surface could be tested, where a possible gradient was suspected. In figure 4.4 the measured values of ultimate tensile strength and elongation to failure are plotted over the sampling depth. As it can be seen in figure 4.4c), a gradient can be found only in the very top layer of the foil up to a sampling depth of about 30µm. The by far more sensitive mechanical property is proven to be the elongation to fracture.

4.3.2 ATR-IR spectroscopy

Figure 4.5 shows the ATR-IR transmittance spectrum of thin sections machined out of the HST-C foil relative to the spectrum of pristine Teflon® FEP thin section. As the spectroscopic data acquired by the ATR set-up gives information only about the material directly at the surface, a depth profile was attempted to be recorded to search for spectroscopic evidence of the measured mechanical degradation.
The measured spectra of the sections HST C-M1_ u, HST C-M1_ l and HST C-M2_ l show big differences relative to the other measurements (e. g. at 1750 cm^{-1}), but the reason for this effect cannot be narrowed down on a possible chemical effect of the ageing of the top surface layer. The new absorption bands are rather originating from some remains of the embedding material. The much lower intensities of the strong C-F stretch absorption peaks are a sign for imperfect coverage of the ATR crystal by the smaller thin sections, machined from the surface region of the HST C foil sample. For these reasons it is not possible to draw conclusions about the chemical composition of the original HST C samples in the surface layer region. The highest C-F absorption peaks were reached by pristine material, but also

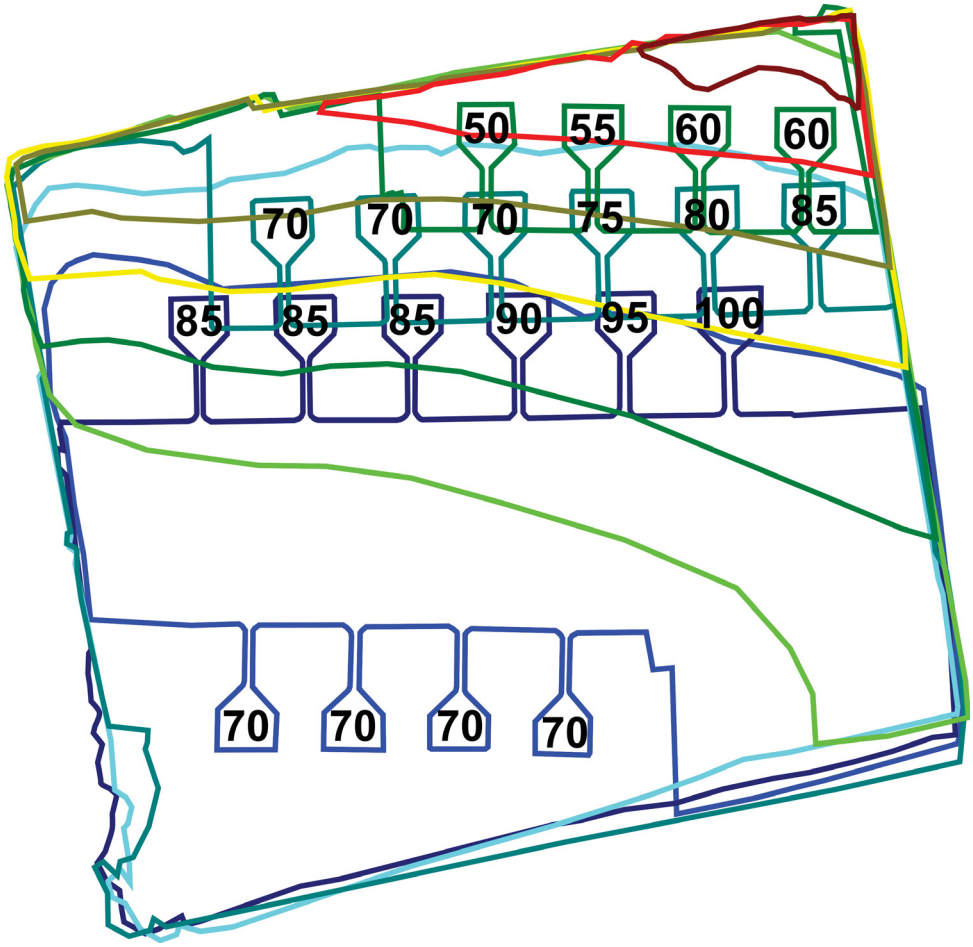

Figure 4.3: Outlines of the aligned thin sections of the sample HST A with the reconstructed average sampling depth (in µm) noted in the head of tensile specimens.

measurements of the HST C thin sections taken from the “bulk region” of the foil show very similar spectra. Within the accuracy of the method no differences were observed, indicating that no new types of chemical bonds are present.

4.3.3 Raman spectroscopy

Raman spectra were acquired from thin sections of samples HST C from the solar facing and HST G from the anti solar facing side of the SADA MLI (see figure 4.6). All three collected spectra show the same typical features of FEP (see section 2.3.2 on page 22) and stand for the absence of new chemical bonds. A clear difference is visible in the baseline shift and the smoothness of the acquired data of HST C-M2 and HST C-M4 relative to HST G-M5. These features can possibly be signs for degradation, but no specific conclusions can be drawn.

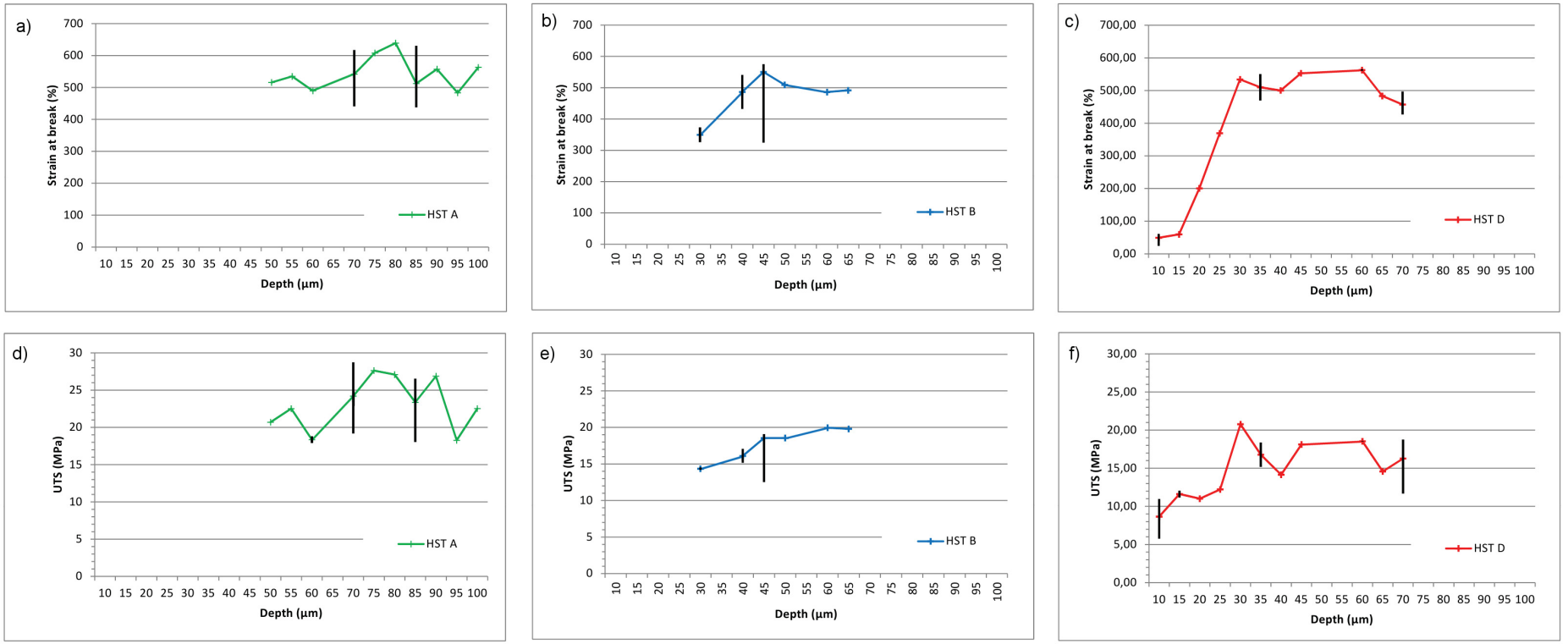

Figure 4.4: Test results from foil samples HST A, HST B and HST C resolved over the thickness of the foil a), b) and c) show the measured strain at fracture. d), e), f) show the measured ultimate tensile strength

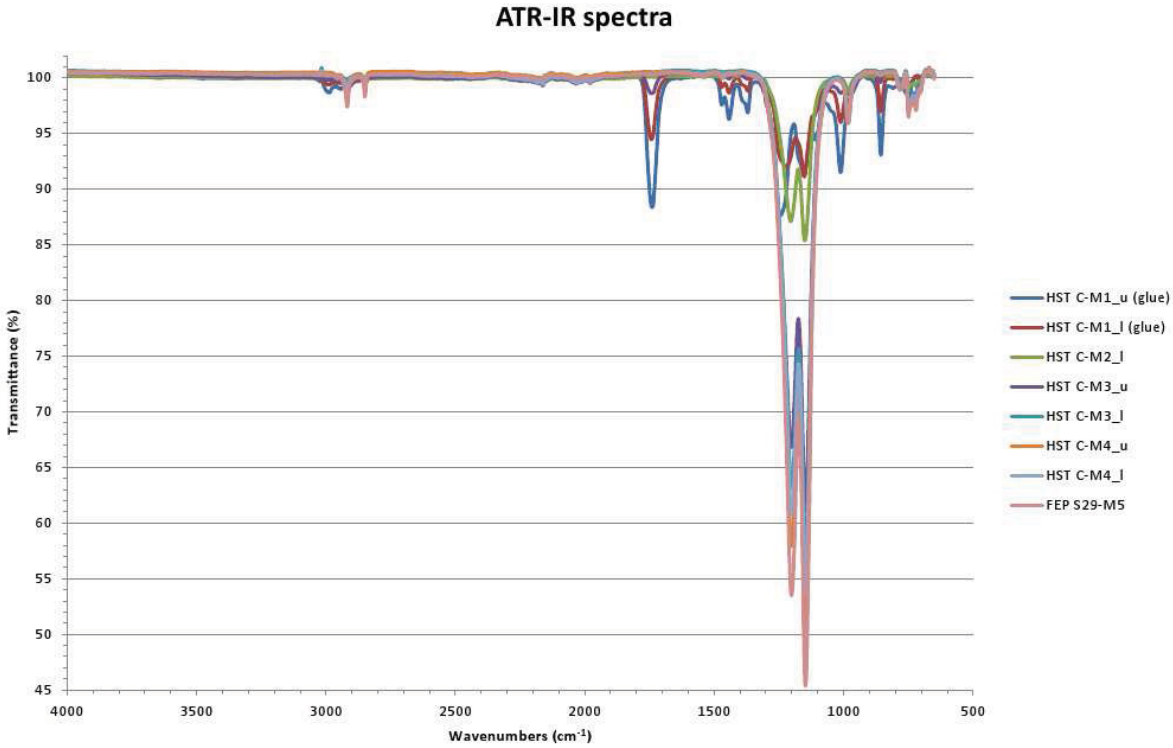

Figure 4.5: ATR-IR spectra of aged material from sample HST-C, referring to the solar facing side of the SADA MLI compared with pristine FEP (sample FEP S29-M5). The numbers after the capital letter M in the samples names are counters for the thin sections starting from the top surface of the material. Indices *u* and *l* stand for the *upper* and *lower* surface of the thin sections, respective.

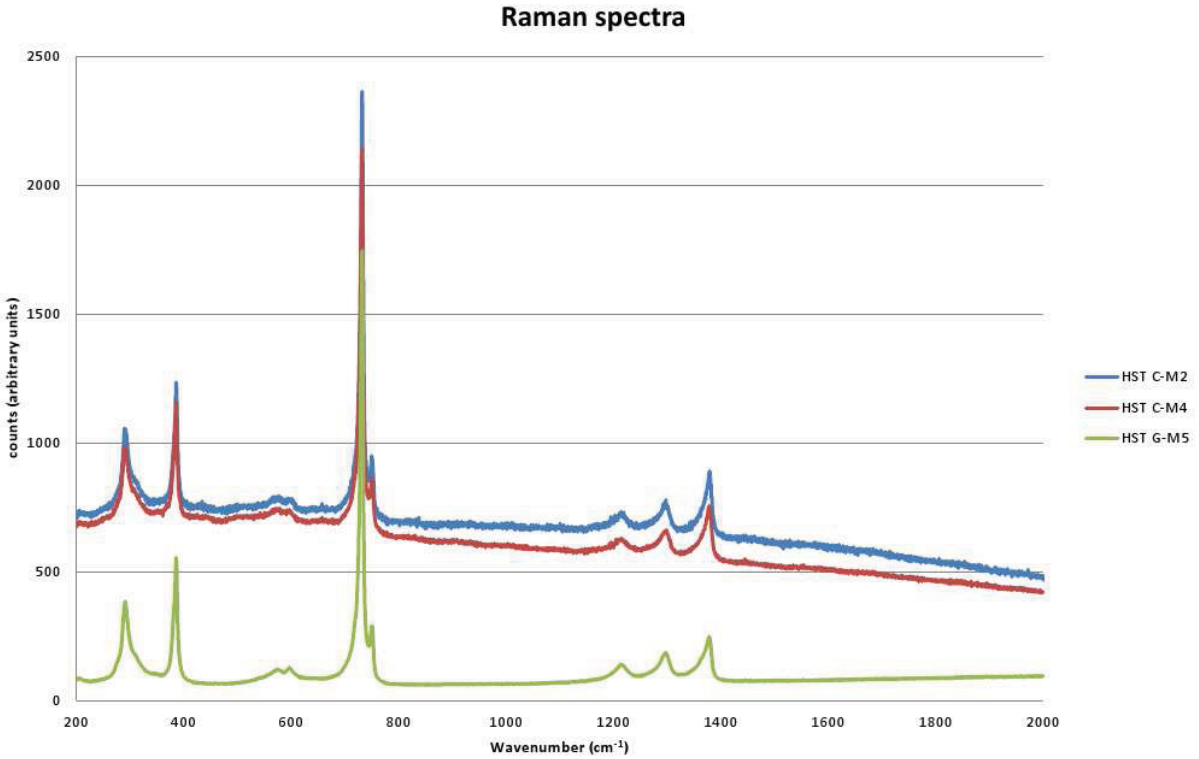

Figure 4.6: Raman spectra of aged material from positions HST-C and HST-G

5 Summary

A sample production technique for tensile specimen in the size range of tens of micrometers was developed. Foil samples were sectioned by a microtome and further processed by ion milling with a masking technique using copper masks of desired geometry. For reproducible geometries it was important to keep the damage to the foil during machining as low as possible. This could be achieved by finding a proper embedding method for microtomy, using a cyanoacrylate adhesive for bonding the foil samples onto a supportive polymer block in the first instance and placing the dumbbell shaped copper masks directly on top of the thin sections in the ion milling system, during further processing.
An important parameter in the specimen production is the amount of processing steps, as it not only determines the overall time needed to get tensile specimens, but each step also represents possiblities of damaging the material. As the sample sizes are in the order of magnitude of big dust particles, cleanliness is also an important issue. The existence of these particles on the surface prior to ion milling can shield the ion beam locally and yield to artefacts and an irregular sample geometry.
Very small pieces of thin sections were difficult to handle during the aligning process of the mask relative to the sections' cutting direction. To be able to use also small-area thin sections, which normally occur close to the surface region of the original foil sample, the thin sections were bonded onto a silicon wafer piece prior ion milling. Relatively low ion beam currents were chosen during ion milling, to limit the heating of the thin section due to dissipated kinetic energy of ions.
Samples machined out of pristine material, were used to assess the reproducibility of tensile test data from macroscopic tensile tests. Thereby, it was found, that the specimens with the tensile direction aligned parallel to the cutting direction in the microtome were showing stress-strain-curves, as known from macroscopic tests. On the other hand samples with an inclination of 45° and 90° between the cutting direction and the tensile direction did fail with significantly lower elongation at fracture values. A possible explanation for these findings is, that the grooves at the surface originating from cutting with an imperfect knife, are inclined perpendicular to the tensile direction and thus acting as notches. But as FEP is a very ductile material, this effect is expected to be very small. Another reason is more problematic: the inducement of residual stresses due to high shear stresses in the microtome (causing also the curling of some thin sections), in combination with stress relaxation during ion milling. When supportive material is removed by ion milling around the forming tensile specimen, the remaining material is free to move from underneath the mask. However, this problem could be solved by aligning samples always along the cutting direction and placing the mask directly on top of the thin section during ion milling. Thus, there is no gap between specimen and mask.
For the tensile testing of space exposed FEP foil samples, the developed sample preparation technique was used to obtain thickness resolved information about the mechanical properties of aged material. Samples from three different solar facing positions of the SADA MLI were prepared. The determination of the sampling depth was carried out graphically by the reconstruction of the original foil sample out of its thin sections.

Tensile experiments of a sample, which was removed from directly next to an in orbit grown crack show a strong reduction of the elongation to failure close to the surface of the original sample. Material at larger depths (seen from the space facing surface) are showing mechanical behaviour scattering around a constant value. It was not possible to test the other two foil samples as close to the surface due to difficulties during sample preparation, but the tensile properties in the 'bulk' of those foil samples also did not show significant gradients in mechanical properties.

This behaviour can be explained by the existence of an embrittled layer, backed up by material with nearly pristine behaviour. The surface layer encountered an environment of AO and absorbed high X-ray and γ radiation with small attenuation lengths and UV light of wavelengths, which are capable of breaking bonds in the polymer chain. This exposure could cause chain scissioning in a thin layer and etching of the surface. The partly crystalline polymer would evolve towards a higher degree of crystallinity and thus lead to embrittlement. Scanning thermal microscopy, another test method giving direct information about the chemical degradation of this small volumes of material, was utilized by H. Fischer and C. O. A. Semprimoschnig and lead also to the conclusion of the formation of a strongly embritteled surfac [32].

ATR-IR spectroscopy and confocal Raman microspectroscopy did not show significant signs of ageing. As even the longest living radicals can be considered as decayed due to more than 11 years of storage after retrieval from space environment, no signals from new chemical bonds are to be expected [26]. Chemical bonds with oxygen are expected only in the very first few atomic layers of the material, where a reaction with AO could have taken place, but exactly that layer was partly contaminated by the embedding material (cyanoacrylate), so that no reliable information could be gathered from those samples. The change in crystallinity and in molecular mass can not be detected via spectroscopic techniques, therefore thermal tests would be necessary.

As an outlook it would be interesting to utilize scanning thermal microscopy on thin sections, to locally resolve differences in the thermal properties of FEP and provide another tool to measure the extent of the embrittled surface layer.

6 List of Symbols

6.1 Roman Symbols and Abbreviations

AO . . . . . Atomic Oxygen

A_P . . . . . Projected surface area of a spacecraft in the direction of a planet [m^2]

A_S . . . . . Projected surface area of a spacecraft in the direction of the Sun [m^2]

A_{SC} . . . . . Total surface area of a spacecraft

Ar . . . . . Argon

ATR . . . . . Attenuated Total Reflectance

AU . . . . . Astronomical unit $1.496 \cdot 10^{11}$ m

c . . . . . velocity of light [m/s^2]

COSTAR . . . Corrective Optics Space Telescope Axial Replacement

ESA . . . . . European Space Agency

ESH . . . . . Equivalent sun hours

$E_{\lambda,T}$ . . . . . Energy of the specific radiation of a black body [W/m^3sr]

F_{12} . . . . . View factor

ESTEC . . . . European Space Technology and Research Centre

F_{ij} . . . . . Radiative view factor

FEP . . . . . Fluorinated Ethylene Propylene

FIB . . . . . Focussed Ion Beam

GEO . . . . . Geosynchronous Orbit

h . . . . . Planck constant $6.626 \cdot 10^{-34}$ Js

HFP . . . . . Hexafluoropropylene

HST . . . . . Hubble Space Telescope

IR . . . . . Infrared

k_B . . . . . Constant of Boltzmann $1.38 \cdot 10^{-23}$ J/K

LEO . . . . . Low Earth Orbit

MEMS . . . . . Microelectromechanical System

MEO . . . . . Mid Earth Orbit

MLI . . . . . Multi Layer Insulation

NASA . . . . . National Aeronautics and Space Administration

PMMA . . . . . Poly(methyl methacrylate)

PS . . . . . Polystyrene

PTFE . . . . . Polytetrafluoroethylene

q . . . . . Energy radiated by a body [W/m^2]

Q_A . . . . . Intensity of the radiation from albedo [W/m^2]

Q_i . . . . . internal power dissipation of spacecraft [W/m^2]

Q_P . . . . . Intensity of the radiation from a planet [W/m^2]

Q_S . . . . . Intensity of the radiation from the Sun [W/m^2]

RT . . . . . Room Temperature

SADA . . . . . Solar Array Drive Arm

SA2 . . . . . HST's second pair of solar arrays

SEM . . . . . Scanning electron microscopy

SM3A . . . . . third HST servicing mission

SM3B . . . . . fourth HST servicing mission

TEM . . . . . Transmission Electron Microscopy

TFE . . . . . Tetrafluoroethylene

UTS . . . . . Ultimate tensile strength

UV . . . . . Ultra violet radiation ($\lambda =$ 400 - 100 nm)

VDA . . . . . Vapour Deposited Aluminium

Vis . . . . . Visible part of the light spectrum ($\lambda =$ 700 - 400 nm)

VUV . . . . . Vacuum ultra violet radiation ($\lambda =$ 200 - 10 nm)

6.2 Greek Symbols and Abbreviations

α . . . . . Absorptance

α . . . . . clearance angle

β . . . . . knife angle

γ . . . . . rake angle

ϵ . . . . . Emittance

λ . . . . . wavelength [nm]

ρ . . . . . Reflectance

σ . . . . . Stefan-Boltzmann constant 5.67 $\cdot$ 10^{-8} Wm^{-2-4}]

τ . . . . . Transmittance

ν_0 . . . . . Frequency of incoming electromagnetic radiation

ν_R . . . . . Frequency of scattered light

7 References

[1] Homepage Hubble Space Telescope. http://hubblesite.org. http://hubblesite.org, 2014. [Online; accessed 03/June/2014].

[2] NASA Glenn Research Center. http://www.nasa.gov. http://www.nasa.gov/centers/glenn/news/pressrel/1999/99_97.html, 2014. [Online; accessed 05/June/2014].

[3] G. B. Field and D. Goldsmith. *The Space Telescope, Eyes above the Atmosphere*. Contemporary Books Inc, 1990.

[4] ESA Hubble Space Telescope homepage. http://www.spacetelescope.org/. http://www.spacetelescope.org/, 2014. [Online; accessed 05/June/2014].

[5] NASA homepage. http://www.nasa.gov. http://www.nasa.gov/mission_pages/shuttle/main/index.html, 2014. [Online; accessed 05/June/2014].

[6] J. A. Townsend, P. A. Hansen, J. A. Dever, et al. Hubble Space Telescope Metallized Teflon® FEP thermal Control Materials: On-Orbit Degradation and Post-Retrieval Analysis. *High Performance Polymers*, 11(81), 03 1999.

[7] M. Moser. Investigation of the Behaviour of Metallised Fluorinated Ethylene Propylene under a Simulated Space Environment. Master's thesis, The University of Leoben, Austria, 11 2003.

[8] M. Moser, C. O. A. Semprimoschnig, M. R. J. Van Eesbeek, and R. Pippan. Surface and Bulk Degradation of Teflon® FEP Retrieved from the Hubble Space Telescope Solar Arrays. *High Performance Polymers*, 20(429), 01 2008.

[9] Federation Aeronautique Internationale (FAI) homepage. http://fai.org. http://www.fai.org/icare-records/100km-altitude-boundary-for-astronautics, 2014. [Online; accessed 12/June/2014].

[10] P. Fortescue, John Stark, and Graham Swinerd, editors. *Spacecraft Systems Engineering 3rd Edition*. Wiley, 07 2010.

[11] E. M. Silverman. Space Environmental Effects on Spacecraft: LEO Materials Selection Guide Part 1. Technical report, NASA Contractor Report 4661, 08 1995.

[12] E. M. Silverman. Space Environmental Effects on Spacecraft: LEO Materials Selection Guide Part 2. Technical report, NASA Contractor Report 4661, 08 1995.

[13] National Renewable Energy Laboratory. Solar Spectra: Standard Air Mass Zero. http://rredc.nrel.gov/solar/spectra/am0/ASTM2000.html, 2014. [Online; accessed 13/June/2014].

[14] D. Romagnoli and S. Theil. De-orbiting satellites in LEO using solar sails. *Journal of Aerospace Engineering, Sciences and Applications*, 4(2):49–59, 04 2012.

[15] M. Alonso and E. J. Finn. *Quantenphysik*. Addison-Wesley Publishing Company, 2nd edition, 1990.

[16] R. Marek and K. Nitsche. *Praxis der Wärmeübertragung*. Hanser, 2nd edition, 2010.

[17] J. Scheirs, editor. *Modern Fluoro Polymers*. Wiley, 1997.

[18] J. G. Drobny. *Technology of Fluoropolymers*. CRC, 2001.

[19] E. I. duPont de Nemours & Co. Dupont fep properties bulletin. http://docs-europe.electrocomponents.com/webdocs/065a/0900766b8065a8bd.pdf. [Online; accessed 15/June/2014].

[20] A. Milintchouk and M. Van Eesbeek. Some Aspects of Degradation of FEP Teflon Material Under the Action of VUV, the Sun and Ground Test VUV Facilities. In J. I. Kleinman and R. C. Tennyson, editors, *Proceedings of ICPMSE-4*. Kluwer Academic Publishers, 2001.

[21] J. F. Rabek. *Photodegradation of Polymers*. Springer, 1996.

[22] J. A. Townsend, P. A. Hansen, and M. W. McClendon. Ground-based testing of replacement thermal control materials for the Hubble Space Telescope. Technical report, NASA, 1999.
[23] P. R. Young and W. S. Slemp. An Analysis of LDEF-Exposed Silvered FEP Teflon Thermal Blanket Material. Technical report, NASA, 12 1991.
[24] V. E. Skurat, E. A. Barbashev, I. A. Dorofeev, et al. The Separate and Compined Effects of VUV Radiation and Fast Atomic Oxygen on Teflon® FEP and Silicon Carbide. In *Proceedings of the 7th International Symposium on Materials in Space Environment*, 1997.
[25] *Degradation of Teflon PTFE and FEP exposed to FAR-Ultraviolet Radiation*, 1994.
[26] J. S. Forsythe and D. J. T. Hill. The radiation chemistry of fluoro polymers. *Progress in Polymer Science*, 25:101 – 136, 10 1999.
[27] Z. X. Zhen. Long lived fluoropolymeric radicals in irradiated fluoropolymer powders at room temperature. *Radiation Physics and Chemistry*, 35:194 – 198, 1990.
[28] K. K. de Groh, J. A. Dever, A. Snyder, S. Kaminski, et al. Solar Effects on Tensile and Optical Properties of Hubble Space Telescope Silver-Teflon® Insulation. Technical Memorandum TM-2006-214336, NASA, 10 2006.
[29] J. S. Jones, J. A. Sharon, J. S. Mohammed, and K. J. Hemker. Small-scale mechanical characterization of space exposed fluorinated ethylene propylene recovered from the Hubble Space Telescope. *Polymer Testing*, 2013.
[30] *Materials Analysis of Space Retrieved Materials from the Hubble Space Telescope*, 10th ISMSE, 2006.
[31] S. Wurster. Nanoindentation of aged FEP retrieved from the Hubble Space Telecope. ESA Contractor Report, 2012.
[32] H. Fischer and C. O. A. Semprimoschnig. Durability of Polymeric Materials in Space: Application of Scanning Thermal Microscopy. *Journal of Spacecraft and Rockets*, 46(1):45–50, 01 2009.
[33] T. Katoh and Y. Zhang. High aspect ratio micrommachining by synchrotron radiation direct photo-etching. *Microsystem Technologies*, 4:135–138, 1998.
[34] L. P. Lee, S. A. Berger, D. Liepmann, and L. Pruitt. High aspect ratio polymer microstructures and cantilevers for biomems using low energy ion beam and photolithography. *Sensors and Actuators*, 71:144–149, 04 1998.
[35] G. H. Michler. *Electron Microscopy of Polymers*. Springer, 2008.
[36] Leica Microsystems. Leica RM2255 Manual.
[37] Hitachi High Technologies America Inc. E-3500 ion milling system manual.
[38] M. Smolka, C. Motz, T. Detzel, W. Robl, T. Griesser, A. Wimmer, and G. Dehm. Novel temperature dependent tensile test of freestanding copper thin film structures. *Review of Scientific Instruments*, 83, 05 2012.
[39] T. Lippert. Laser Application of Polymers. *Advances in Polymer Science*, 168:51 – 246, 2004.
[40] B. Yang, C. Motz, W. Grosinger, W. Kammrath, and G. Dehm. Tensile behaviour of micro-sized copper wires studied using a novel fibre tensile module. *International Journal of Materials Research*, 99(7):716 – 724, 2008.
[41] P. W. Atkins and J. de Paula. *Physikalische Chemie*. Wiley, 4 edition, 2007.
[42] R. E. Hummel. *Electronic Properties of Materials*. Springer, 3 edition, 2005.
[43] G. Kämpf. *Characterization of Plastics by Physical Methods*. Hanser, 1986.
[44] H. Lobo and J. V. Bonilla, editors. *Handbook of Plastics Analysis*, volume 68 of Plastics engineering. CRC Press, 2003.
[45] H. Günzler and H. U. Gremlich. *IR-Spektroskopie*. Wiley-VCH, 4 edition, 2003.
[46] P. I. Okagbare and M. D. Morris. Polymer-capped fiber-optic Raman probe for non-invasive Raman spectroscopy. *Analyst*, pages 77 – 81, 01 2012.

8 Appendix

8.1 Depth reconstruction

8.2 Tensile test plots

Figure 8.1: Outlines of the aligned thin sections of the sample HST B with the reconstructed average sampling depth (in µm) noted in the head of tensile specimens.

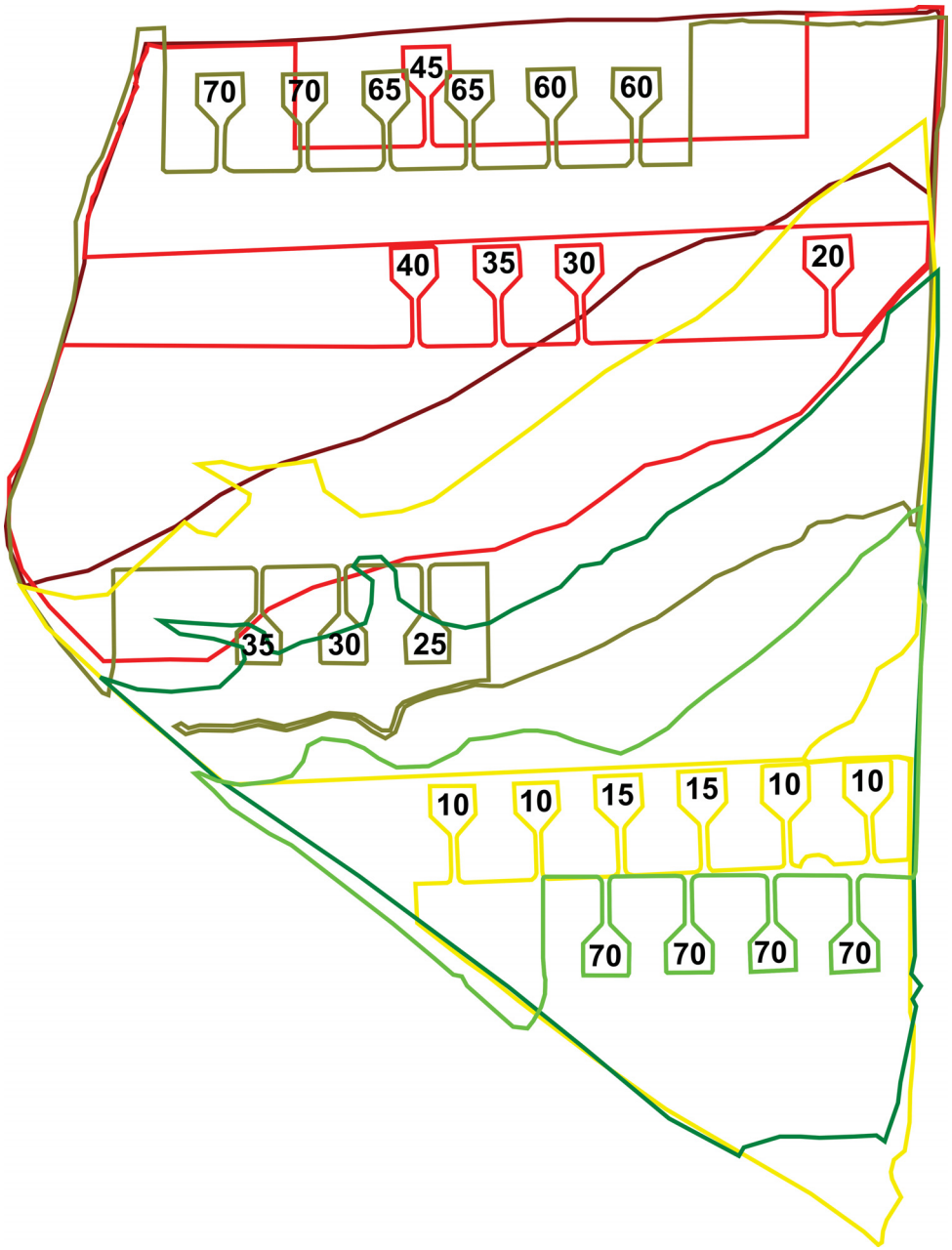

Figure 8.2: Outlines of the aligned thin sections of the sample HST D with the reconstructed average sampling depth (in µm) noted in the head of tensile specimens.

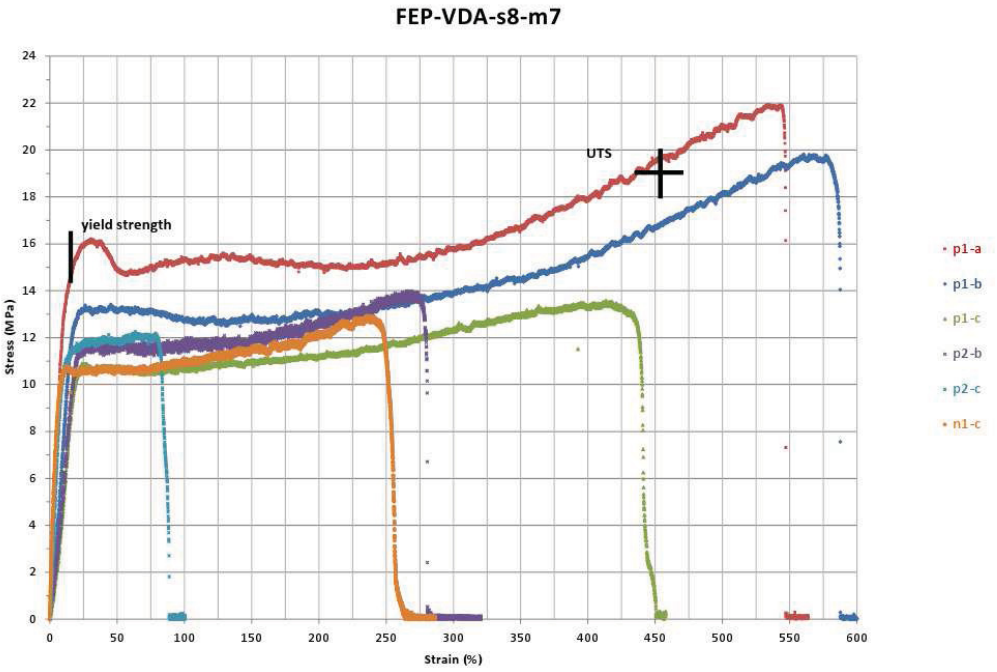

Figure 8.3: The first successful tensile tests with 30µm thick and wide tensile specimens machined out of pristine FEP/VDA foil. In the specimen names ’n’ means, that the tensile direction was perpendicular to the microtome cutting direction, whereas ’p’ means that the tensile direction was parallel to the microtome cutting direction

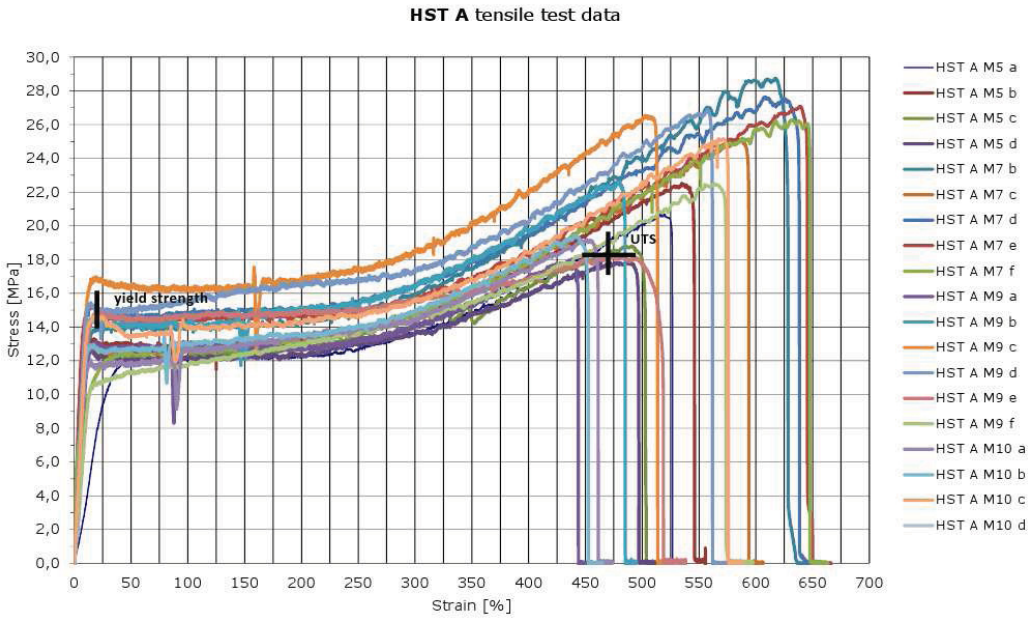

Figure 8.4: Tensile test plots of the specimens machined out of the foil sample HST A.

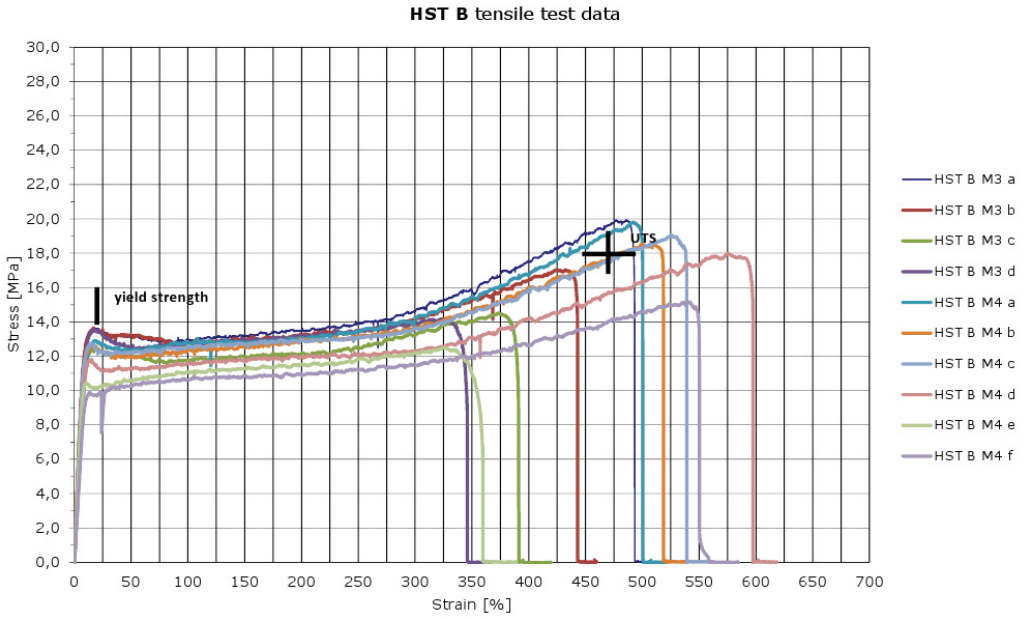

Figure 8.5: Tensile test plots of the specimens machined out of the foil sample HST B.

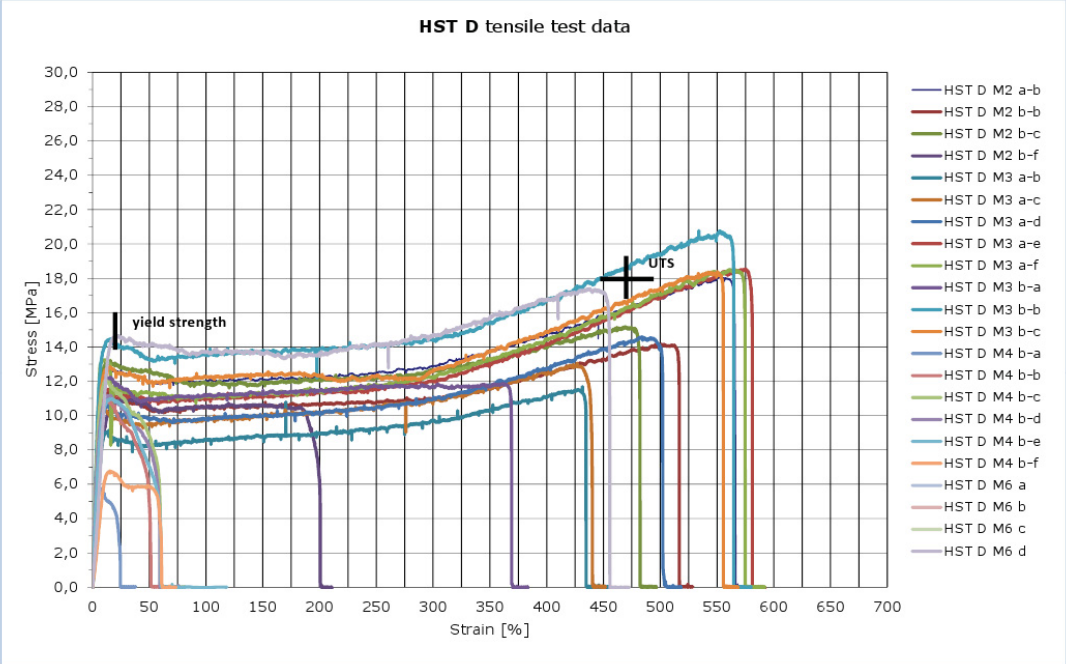

Figure 8.6: Tensile test plots of the specimens machined out of the foil sample HST D. Note the big difference in elongation to failure values of the samples, which are taken from closely under the original surface.